

ARID1B is a Dosage-sensitive Regulator of Polycomb Repressive Complex Distribution and HOX Gene Regulation in Patient-derived Neural Progenitors

Gerald Crabtree (✉ crabtree@stanford.edu)

Stanford University <https://orcid.org/0000-0001-9685-7911>

Esther Son

Stanford University

Andrey Krokhotin

Howard Hughes Medical Institute, Stanford School of Medicine

Sai Gourisankar

Department of Chemical Engineering, Stanford School of Engineering

Chiung-Ying Chang

Howard Hughes Medical Institute, Stanford School of Medicine

Article

Keywords: Autism, intellectual disability, haploinsufficiency, chromatin, SWI/SNF, BAF complexes

Posted Date: October 29th, 2021

DOI: <https://doi.org/10.21203/rs.3.rs-959800/v1>

License:  This work is licensed under a Creative Commons Attribution 4.0 International License.

[Read Full License](#)

1 **ARID1B is a Dosage-sensitive Regulator of Polycomb Repressive Complex**
2 **Distribution and HOX Gene Regulation in Patient-derived Neural Progenitors**

4 Esther Y. Son^{1,2,3*}, Andrey Krokhotin^{1,2,*}, Sai Gourisankar^{1,4}, Chiung-Ying Chang^{1,2}, Gerald R.
5 Crabtree^{1,2}

7 **Affiliations:**

8 ¹Howard Hughes Medical Institute, Stanford School of Medicine

9 ²Department of Pathology, Stanford School of Medicine

10 ³Department of Ophthalmology, University of California San Francisco

11 ⁴Department of Chemical Engineering, Stanford School of Engineering

12 *Equal contribution

13 **Keywords:** Altism, intellectual disability, hploinsufficiency, chromatin, SWI/SNF, BAF
14 complexes

15

16

17

18 **Abstract**

19 Recent unbiased exome and whole-genome sequencing studies have identified *ARID1B* (originally
20 *BAF250b*) as the most frequently mutated gene in human de novo neurodevelopmental disorders
21 and a high confidence autism gene. *ARID1B* is a subunit of the multimeric SWI/SNF or
22 Brg/Brahma-Associated Factor (BAF) ATP-dependent chromatin remodeling complex. Studies of
23 *Arid1b*^{+/−} mice as well as other BAF subunit mutants have found defects in neural progenitor
24 proliferation and activity-dependent neuronal dendritogenesis; however, to date, the molecular
25 impact of *ARID1B* mutations on the human neural lineage has not been investigated. Remarkably,
26 *ARID1B* is required for expression of *HOX* genes, including anterior *HOX* genes necessary for
27 brain development. Despite the high homology with *ARID1A* and the fact that *ARID1A* is
28 expressed at about 3-fold higher levels, it is unable to compensate for heterozygous loss of
29 *ARID1B*. These changes in gene expression were paralleled by dosage-sensitive altered deposition
30 of histone H3 lysine-27 trimethylation (H3K27me3) and histone H2A lysine-119 ubiquitination
31 (H2AK119ub) indicating that an evolutionarily conserved pathway of *HOX* gene regulation
32 underlies the neurodevelopmental defects accompanying *ARID1B* haploinsufficiency. Using
33 FIRE-Cas9, we show that the unmutated *ARID1B* allele can be activated to near normal and
34 potentially therapeutic levels.

35 **INTRODUCTION**

36 The human genome encodes 31 ATP-dependent chromatin regulatory enzymes homologous to
37 yeast SWI2/SNF2. The members of this class investigated to date exert their functions on
38 overlapping aspects of nucleosome dynamics, yet play highly specific biologic roles. The first to
39 be discovered was the yeast SWI/SNF complex^{1,2}, named after its roles in yeast mating type
40 switching and sucrose fermentation. In flies, related complexes containing the Brahma (Brm)
41 ATPase were discovered to suppress mutations in Polycomb repressive complexes (PRC) and to
42 influence development³. In mammals, related Brahma-associated factor (BAF), or mammalian
43 SWI/SNF (mSWI/SNF), complexes consist of 15 to 17 subunits encoded by 29 to 31 genes that
44 are assembled in combinatorial fashion. In the normal development of the mammalian nervous
45 system, BAF complexes exchange subunits to generate neuronal BAF (nBAF) complexes found
46 only in neurons^{4–7}. This switch in subunit composition as cells progress from neural progenitors
47 to neurons is critical for cell cycle exit and maturation^{8,9}. *ARID1B*, the largest core subunit of
48 BAF complexes, is implicated in several neurodevelopmental disorders. Mutations in the *ARID1B*
49 gene were found to be the most common cause of Coffin-Siris syndrome^{10–13}. *ARID1B* is
50 frequently mutated in patients with nonsyndromic intellectual disability^{14,15}, autism spectrum
51 disorder (ASD)^{16–18}, and unclassified neurological developmental disorders¹⁹. Importantly,
52 *ARID1B* is haploinsufficient for normal human neurodevelopment¹⁵, while loss of both alleles
53 leads to early postnatal death in mice²⁰. Genetic surveys of mutations in the normal human
54 population performed on a cohort of 141,456 unrelated individuals revealed that *ARID1B* is
55 intolerant to loss of function mutations in one allele, raising the question of the nature of the dosage
56 sensitive biologic mechanism²¹. Dosage sensitivity of a gene often reflects a rate-limiting
57 biochemical step in a developmental, metabolic, or other pathway and hence can be
58 mechanistically informative.

59 At the molecular level, the BAF complex slides and evicts nucleosomes in vitro in an ATP
60 dependent manner²², thereby creating and maintaining genomic accessibility at its target sites^{23–}
61 ²⁹. BAF is also implicated in regulation of PRC^{3,23,30–32} both directly, through PRC eviction³³, and

64 indirectly, by promoting genome-wide PRC redistribution possibly as a passive result of
65 widespread direct eviction²⁹. PRC eviction is rapid, occurring within minutes of BAF recruitment
66 to endogenous PRC-repressed loci in somatic cells³²⁻³⁴. Oncogenic mutations in the ATPase
67 domain of Brg (SMARCA4) prevent rapid PRC eviction³², and PRC eviction does not appear to
68 be a property of other chromatin regulatory complexes³⁵.

69 In flies, BAF opposes Polycomb-mediated repression at the *HOX* loci, thereby allowing
70 normal topological and temporal development of the body plan³. Intriguingly, some of the clinical
71 characteristics of *ARID1B* patients resemble phenotypes seen upon *HOX* gene inactivation. For
72 example, Coffin-Siris patients are characterized by hypoplasia of the distal phalanx or nail of the
73 fifth and other digits. *HOX* gene groups 11, 12, and 13 control size and number of digits in dose
74 dependent manner. In *HOX* mutant mice, the most commonly observed digit alteration involves
75 reduction in digit size and loss of phalanges³⁶. Similar symptoms were observed in humans
76 carrying mutations in *HOXA13* and *HOXC13*³⁷. Most Coffin-Siris patients have hypotonia, and
77 delayed development of motor skills¹⁰. Reduced muscle strength and deficits in motor skill
78 coordination are also observed in the *Arid1b^{+/−}* mouse model³⁸, and *HOX* genes are important
79 players in the differentiation of motor neurons, responsible for proper muscle innervation³⁹ and
80 motor skill development⁴⁰.

81 Several *Arid1b* deficient mouse models consistently exhibit neurodevelopmental
82 phenotypes seen in patients with *ARID1B* mutations, including reduced cortical volume and
83 thickness, as well as deficits in learning, memory, and socialization^{20,38,41-43}. Neuron subtype-
84 specific analysis revealed that *Arid1b* mutant mice have decreased numbers of cortical GABAergic
85 interneurons, which shifts the balance between excitatory and inhibitory synapses in the cerebral
86 cortex⁴¹. Remarkably, mice with selective *Arid1b* deletion either in parvalbumin or somatostatin
87 interneurons, two subtypes of inhibitory interneurons, exhibit distinct phenotypes, characterized
88 either by impairment of social interactions or by stereotypic behavior as well as learning and
89 memory dysfunction⁴². Finally, cortical and ventral neural progenitors with homozygous *Arid1b*
90 deletion displayed reduced proliferation rate, altered cell cycle regulation, and increased cell death
91⁴⁴. Recently, ARID1b has been shown to execute its social functions in neurons of the dorsal raphe
92 of adult mice, raising the possibility of effective therapy in adults⁴⁵.

93 Despite these recent advances in recapitulating the human phenotypes in murine models,
94 the molecular function of ARID1B remains unclear and the nature of the presumably rate-limiting
95 biochemical step performed by ARID1B is unknown. To understand the roles of BAF complexes
96 in the development of the human nervous system, we used human induced pluripotent stem cell
97 (iPSC)-derived neural progenitor cells (NPCs) containing inactivating mutations within the genetic
98 context of the *ARID1B* patient. The mutant NPCs exhibited reduced proliferation and increased
99 differentiation, had impaired WNT signaling and reduced binding of SOX family transcription
100 factors and several nuclear receptors. Importantly, the *ARID1B*-mutant human NPCs have striking
101 haploinsufficient deficits in transcription, chromatin accessibility, and PRC placement over the
102 genome. Indeed, the loss of one or two alleles appeared to have very similar effects on gene
103 expression, chromatin accessibility, *HOX* gene activation, and PRC placement over the genome.
104 Our studies suggest that BAF's ability to evict PRC from multiple sites over the genome and
105 redistribute PRC to the four *HOX* loci is a rate-limiting step in the development of the human
106 nervous system. As was previously shown in yeast⁴⁶, the expression level of haploinsufficient
107 genes is tightly regulated, potentially making these genes resistant against attempts to
108 programmatically alter their expression. Nevertheless, we demonstrate that expression of the wild
109 type endogenous *ARID1B* allele can be boosted to compensate for the lack of the expression from

110 the second endogenous allele lost due to deleterious mutations, paving the way for potential
111 therapeutical applications.

112

113 RESULTS

114 **Proliferation of *ARID1B* deficient NPCs is impaired.** Because the phenotypes of *ARID1B*
115 mutations are highly genetically context-dependent, we used an iPSC line derived from a patient
116 with Coffin-Siris syndrome, a neurodevelopmental disorder characterized by intellectual
117 disability, language delay, and social deficits, as well as distinct facial features and hypoplastic
118 fifth fingernails. The patient had a frameshift mutation in exon 12 of the *ARID1B* gene; using
119 CRISPR/Cas9 on the original patient iPSC line ('HET1'), we then derived isogenic iPSC lines
120 with two wild-type copies of *ARID1B* ('WT1' and 'WT2') and isogenic lines with two non-
121 functional copies of the gene (called 'KO1' and 'KO2'). An additional isogenic line heterozygous
122 for *ARID1B* ('HET2') bearing one wild-type allele and a new truncated allele was identified from
123 the pool of CRISPR/Cas9-edited clones (Supplementary Fig. 1a). These efforts gave us a full
124 isogenic series to allow normalization for genetic context. Analysis of *ARID1B* mRNA levels by
125 qRT-PCR showed an approximately 50% and <20% expression in the heterozygous and double-
126 mutant iPSC lines, respectively, relative to their wild-type counterparts (Supplementary Fig. 1b).
127 Western blot revealed that the ARID1B protein was expressed at about 50% of normal in the
128 heterozygous iPSCs (Supplementary Fig. 1c). The mutant iPSCs proliferated at about the same
129 rate as the wild type cells (data is not shown). Upon neuronal induction, the mutant iPSCs
130 generated NESTIN⁺ SOX1⁺ neural progenitors with similar efficiencies as the wild-type
131 (Supplementary Fig. 1d) but showed a mild reduction in proliferative rate (Supplementary Fig.
132 1e).

133

134 ***ARID1B* deficient NPCs exhibit strong haploinsufficient phenotypes and increased
135 differentiation to neurons.** To define the genes dependent upon ARID1B, we carried out RNA-
136 seq studies of the NPCs at day 40 after the start of neuronal induction in iPSCs. The heterozygous
137 and double-mutant samples were seen clustered together, away from wild-type samples (Fig. 1a).
138 Similarly, principal component analysis indicated that the major determinant of variation was the
139 genotype among the independently derived NPCs (Fig 1b). Hundreds of genes were misregulated
140 in *ARID1B* mutant cells as compared to the isogenic wild type (Fig. 1c), while only a few genes
141 were differentially expressed between *ARID1B* heterozygous and double-mutant NPCs
142 (Supplementary Fig. 1f). Gene Ontology (GO) term analysis revealed that the most significant
143 terms associated with genes increased in *ARID1B* mutant NPCs are related to neurogenesis, while
144 significant terms associated with decreased genes include cell proliferation and positive regulation
145 of cell proliferation (Fig. 1d). The previous studies showed that neurogenesis in neural progenitors
146 is accompanied by switching of neural progenitor-specific BAF (npBAF) subunits to neuronal-
147 specific BAF subunits (nBAF)⁶. Indeed, we observed a statistically significant increase in
148 expression of *ACTL6B* (log2FC=1.3, FDR=5.9 10⁻⁴), an nBAF specific subunit. Other nBAF
149 specific subunits (*DPF1*, *DPF3*, *SS18L1*) showed minor but consistent increase in expression,
150 while all npBAF specific subunits (*PHF10*, *DPF2*, *SS18*, *ACTL6A*) exhibited decreased
151 expression. Despite increased neurogenesis in *ARID1B* mutant cells, neuronal progenitors
152 predominated in the cell population, such that the *ACTL6B* neuronal paralog was only expressed
153 at 5% of *ACTL6A*. Specific GO terms associated with upregulated genes include synapse formation
154 and function, axonal guidance, and dendritic development (Fig. 1d). Subunits of the BAF complex

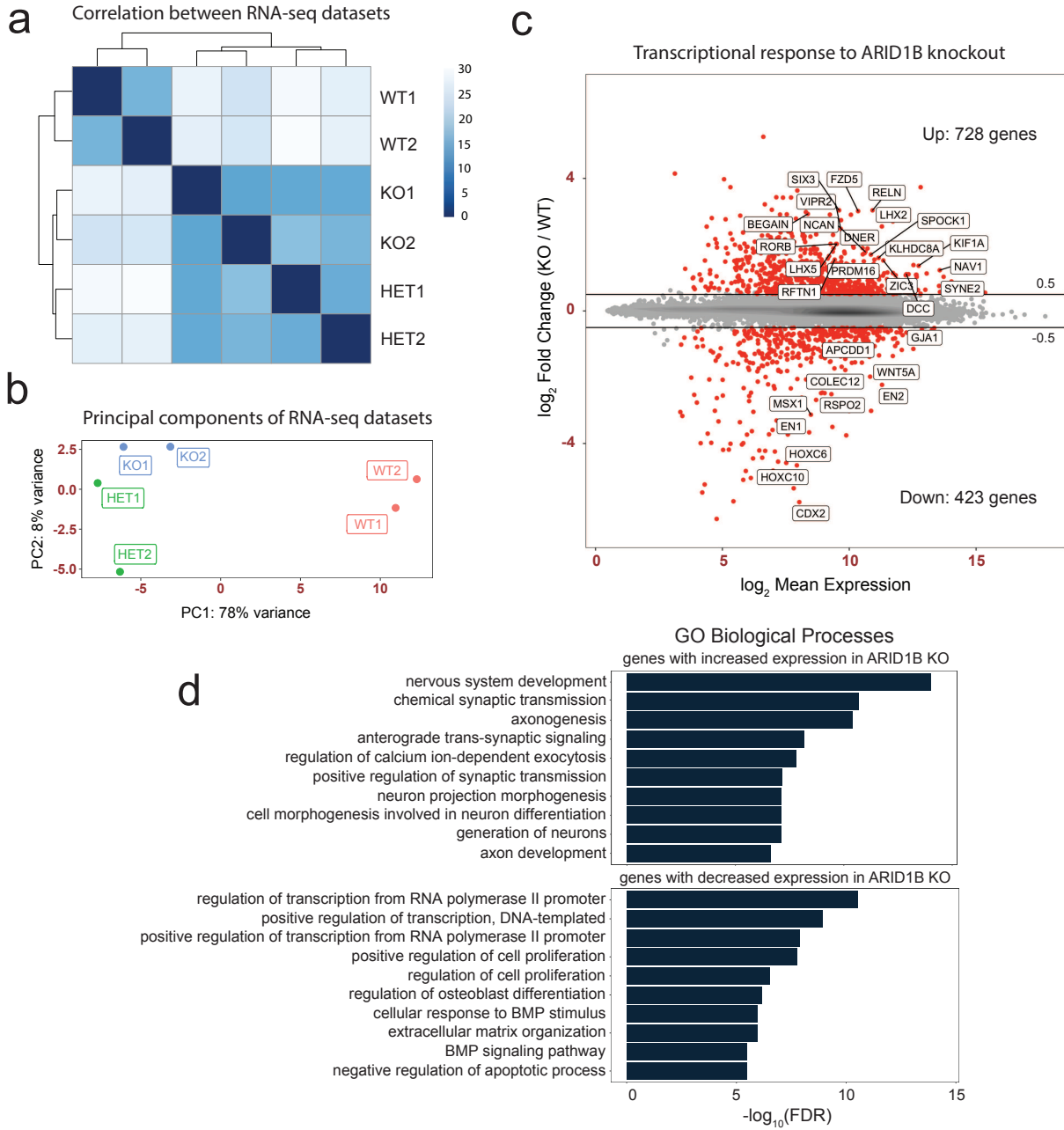


Figure 1: ARID1B dosage-sensitive effect on transcription of NPCs. (a) Correlation between RNA-seq datasets. (b) Principal component analysis of RNA-seq datasets. (c) MA plot showing gene expression changes between ARID1B WT and KO datasets. Genes with $|\log_2 FC| > 0.5$ and $FDR < 0.05$ are colored in red. The top 30 genes with the lowest FDRs are labeled. (d) Gene Ontology Biological Processes enrichments analysis for genes with altered expression in KO NPCs. All results are shown at Day 40 after start of hESCs differentiation to NPCs.

155 have been previously implicated in activity-dependent dendritic outgrowth and synaptogenesis in
 156 mice^{5,47,48}, which speaks to the evolutionary conservation of function in humans. Together, these
 157 results indicate that ARID1B maintains NPCs stemness. Impairment of ARID1B functions causes

158 early differentiation of NPCs to neurons, while wild-type NPCs exhibit neuronal differentiation at
159 later time points.

160

161 **WNT and TGF-β signaling is impaired in *ARID1B* deficient NPCs.** Previous reports implicated
162 ARID1B in regulation of the Wnt signaling pathway, which is mediated through direct interaction
163 between SMRACA4 ATPase subunit of the BAF complex and β-catenin⁴⁹. The effect of ARID1B
164 on Wnt signaling is context-dependent. As an example, the analysis of peripheral lymphocytes
165 from individuals with intellectual disability harboring *ARID1B* mutations as well as in vitro studies
166 in several cancer cell lines demonstrated a repressive role of ARID1B on Wnt/β-catenin signaling
167⁴⁹. The same conclusion was reached in another study on HEK293T and ATDC5 cells, which
168 observed an increase in *AXIN2* and *LEF1* expression upon *ARID1B* knock out⁵⁰. Contrary to these
169 findings, the analysis of gene expression in cerebral cortex of *Arid1b* deficient mice showed that
170 components of the Wnt pathway are downregulated⁴¹. It was also shown that ARID1B is required
171 for induction of *MYC* expression, a target of Wnt/β-catenin signaling, in MC3T3-E1 pre-osteoblast
172 cell line⁵¹. Finally, decreased nuclear localization of β-catenin was observed in *Arid1b* deficient
173 neurons⁴⁴. Surprisingly, deletion of *ARID1B* in human neural progenitors had a programmatic,
174 but complex role in WNT regulation resulting in increased expression of some components of the
175 WNT pathway and decreased expression of others (Supplementary Fig. 1g). Remarkably, we
176 found that many of the genes whose expression was reduced are known downstream WNT targets,
177 including *AXIN2*, *LEF1*, *MYC*, *NKDI* and *WNT1*. This is consistent with the finding that BAF is
178 required in murine neural progenitors for effective Wnt signaling⁸. In contrast, genes with
179 increased expression are enriched for negative regulators of the Wnt pathway, including APC2, a
180 component of the β-catenin destruction complex, SFRP1, multiple cadherins, including E-cadherin
181 and multiple protocadherins⁵². Thus, ARID1B exerts a programmatic and positive role in WNT
182 signaling in neural progenitors.

183 TGF-β is another signaling pathway whose components are downregulated in *ARID1B*
184 deficient NPCs (Supplementary Fig. 1g). This is consistent with previous observations that BAF
185 complexes are required for activation of TGF-β downstream target genes⁵³, and that Smad2/3, the
186 mediators of TGF-β signal transduction, directly interact with BAF complex subunits^{53,54}.

187

188 **Loss of accessibility is observed at BAF binding sites in *ARID1B* deficient NPCs.** We used
189 ATAC-seq to investigate the role of ARID1B on producing genomic accessibility in neural
190 progenitors. Again, the major component of variability among data samples was the genotype,
191 with the heterozygous and double-mutant samples clustered together (Fig. 2a,b). Hundreds of
192 ATAC-seq peaks were significantly altered between wild-type and mutant NPCs (Fig. 2c). GO
193 term analysis revealed that peaks with decreased accessibility in the *ARID1B* mutants significantly
194 associate with genes involved in negative regulation of neurogenesis and neuron differentiation
195 (Fig. 2d). This is consistent with our RNA-seq data on increased differentiation of mutant *ARID1B*
196 NPCs to neurons. We note that peaks with altered accessibility are depleted from promoter regions
197 as compared to the total fraction of accessibility peaks found in promoters (Fig. 2e). To explore

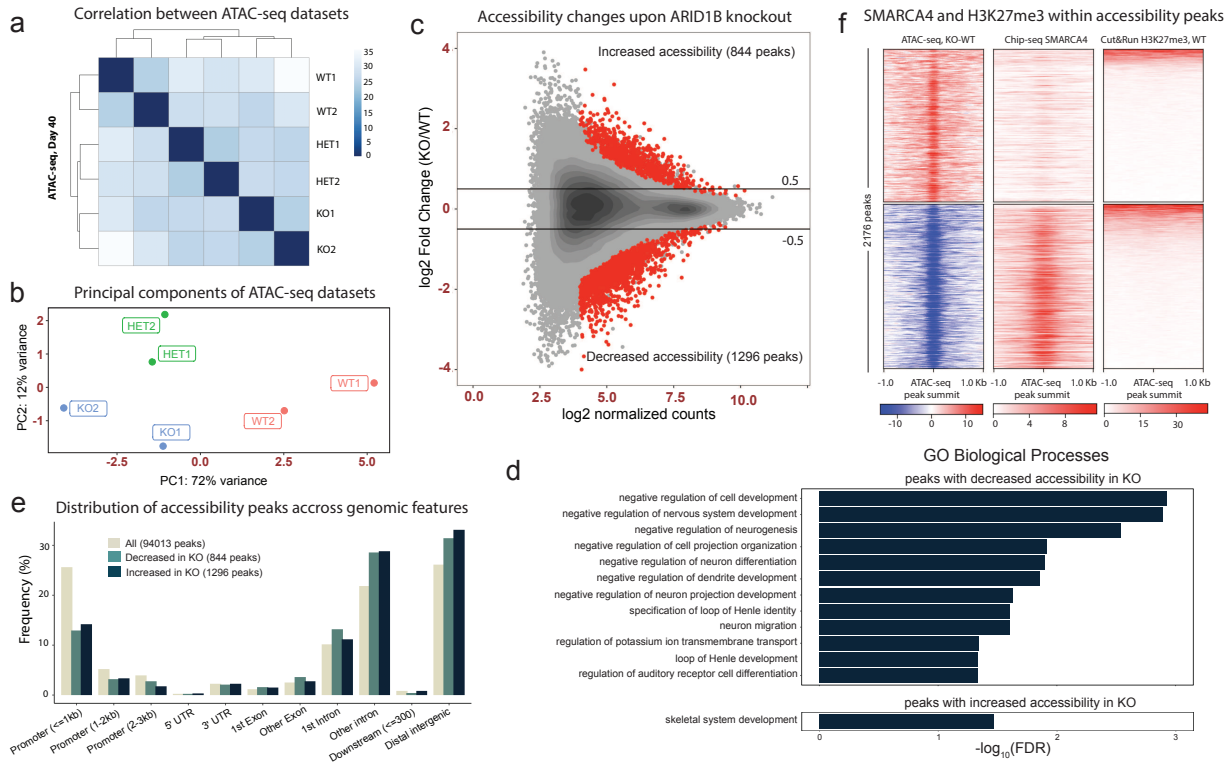


Figure 2: ARID1B promotes accessibility at BAF binding sites. (a) Correlation between ATAC-seq datasets. (b) Principal component analysis of ATAC-seq datasets. (c) MA plot showing changes of accessibility between ARID1B WT and KO datasets. Peaks with $|\log 2FC| > 0.5$ and $FDR < 0.1$ are colored in red. (d) Gene Ontology Biological Processes associated with ATAC-seq peaks altered upon ARID1B knock out. (e) Distribution of ATAC-seq peaks over genomic features. (f) A heatmap showing association between accessibility changes ($FDR < 0.1$), SMARCA4 binding and H3K27me3 marks around summits of ATAC-seq peaks. All results are shown at Day 40 after start of hESCs differentiation to NPCs.

198 the relationship between accessibility changes and BAF occupancy we utilized SMARCA4
 199 chromatin immunoprecipitation (ChIP)-seq dataset previously collected in the wild-type human
 200 NPCs⁵⁵. Strikingly, we found that peaks with decreased accessibility in *ARID1B* mutants are
 201 strongly associated with BAF binding in the wild-type NPCs, which is not the case for peaks with
 202 increased accessibility (Fig. 2f). This result is consistent with a role of BAF complexes in creating
 203 and maintaining genomic accessibility^{27,28}. Another important role of BAF is to counteract
 204 repression mediated by PRC, which is achieved by direct and ATP-dependent PRC eviction^{32,33}.
 205 However, accessibility changes induced by BAF loss only partially overlap with H3K27me3
 206 marked regions (Fig. 2f), which demonstrates that most of ARID1B action is not directly related
 207 to PRC redistribution.

208
 209 **Transcription factor networks are heavily mis-regulated upon ARID1B loss: SOX family**
 210 **transcription factors and family of nuclear receptors are among the most affected.** To explore
 211 the association between accessibility and transcription factor (TF) binding, we used a modified

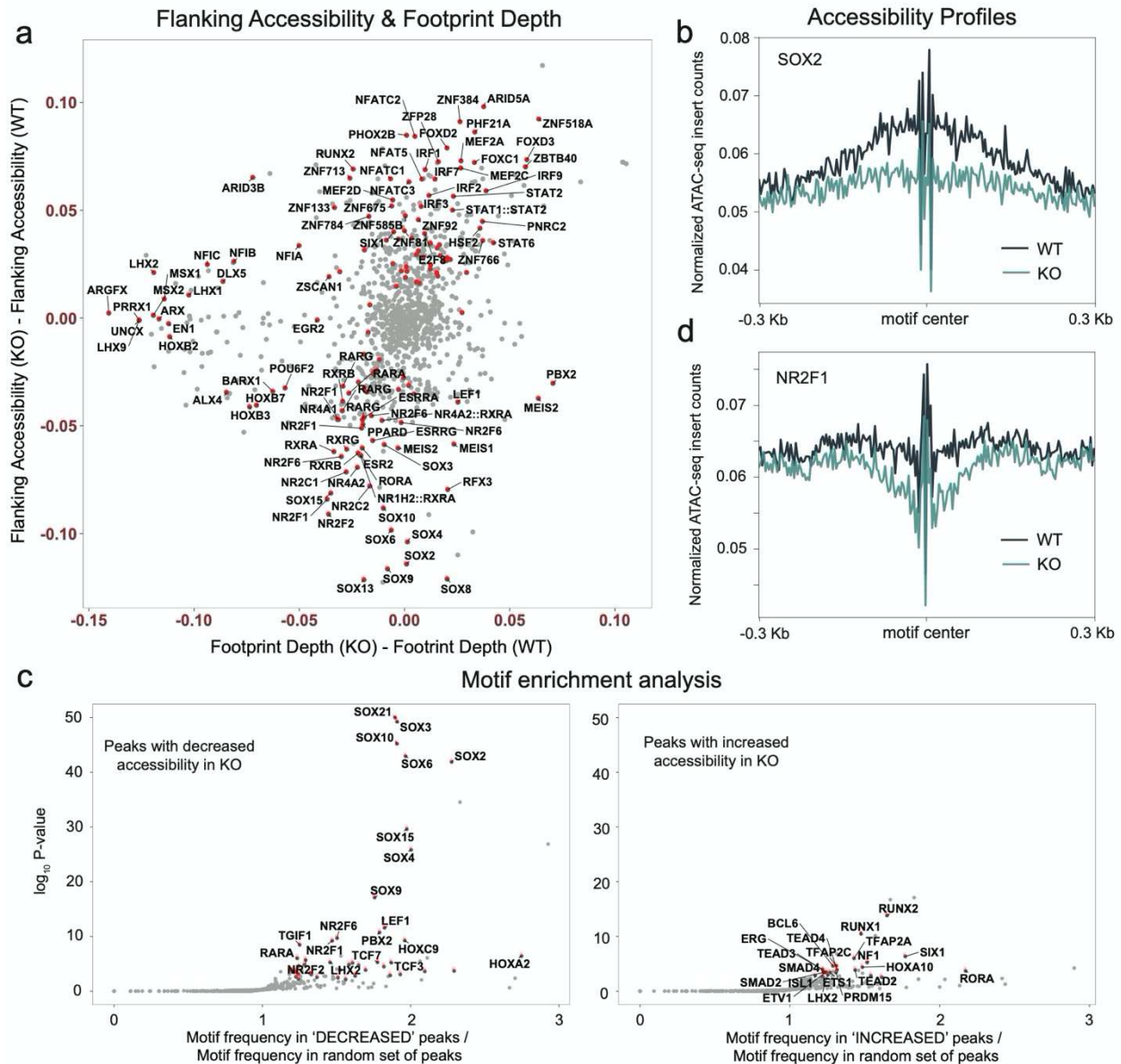


Figure 3: ATAC-seq accessibility profiling reflects extensive perturbation of transcription factor regulatory networks. (a) Changes of Flanking Accessibility and Footprint Depth between ARID1B WT and KO. Motifs with $FDR < 0.05$ corresponding to genes with at least minimal expression at NPCs are colored in red. The minimal expression is defined from RNA-seq data as expression exceeding a random threshold in 50 normalized counts calculated by DESeq2⁸³. (b) Accessibility profile of SOX2 and (c) NR2F1 (COUP-TF I). (d) Motif enrichment analysis found within peaks with decreased accessibility (*left*) and increased accessibility (*right*). All results are shown at Day 40 after start of hESCs differentiation to NPCs.

version of an approach quantifying TF binding based on flanking accessibility, a measure of accessibility in the region adjacent to the TF binding site, and footprint depth, a measure of protection from Tn5 access by the TF^{56,57}. A change in flanking accessibility and footprint depth reflects the effect of *ARID1B* genomic deletion on TF binding (Fig. 3a and Supplementary Fig.

216 2b). A group of SOX TFs exhibited the largest loss of flanking accessibility. In particular, SOX2
217 and SOX3, which are involved in the generation and maintenance of neural stem and progenitor
218 cells, exhibited loss of flanking accessibility, which is confirmed by comparing their accessibility
219 profiles between wild-type and *ARID1B* mutant NPCs. (Fig. 3b, Supplementary Fig. 2c). This
220 result is supported by enrichment analysis of TF binding motifs present within peaks with
221 decreased accessibility. SOX TFs are the most enriched motifs compared to all other motifs
222 enriched in peaks with either decreased or increased accessibility (Fig. 3c).

223 Multiple nuclear receptors expressed in NPCs represent another group of TFs affected by
224 *ARID1B* deletion. This group includes NR2F1 (COUP-TF I), NR2F2 (COUP-TF II), RARA,
225 RARG, RORA, NR2F6, NR4A2, NR1H2, NR2C1, NR2C2, RXRA, and RXRB. Depending on
226 context and ligand binding status, nuclear receptors can either be repressors or activators. To
227 elucidate potential repressor or activator status of these nuclear receptors, we looked at their
228 accessibility profiles (Fig. 3d and Supplementary Fig. 2d-g). We found that all accessibility
229 profiles have a deep valley in the vicinity of the nuclear receptor binding sites, which suggests
230 these nuclear receptors reduce accessibility and promote chromatin compaction, thus playing a
231 repressive role. Remarkably, we found that upon *ARID1B* deletion, these nuclear receptors became
232 even stronger repressors, which is reflected in reduced accessibility around their binding sites.
233 Thus, in the wild-type NPCs, *ARID1B* counteracts repression induced by nuclear receptors.

234 Accessibility profiles of several other TFs are affected both by heterozygous and
235 homozygous *ARID1B* loss of function mutations (Supplementary Data 1), which includes MEIS2
236 (Supplementary Fig. 2h), LEF1, SIX1, ARX, ZEB1, LHX1, and LHX2. LEF1, a known
237 downstream WNT target, has reduced flanking accessibility and increased footprint depth,
238 suggesting reduced LEF1 binding. This is consistent with decrease in *LEF1* transcription observed
239 in *ARID1B* heterozygous and double-mutant NPCs, and further supports our observation that
240 *ARID1B* positively regulates WNT signaling in neural progenitors.

241 While the number of peaks with significant changes in accessibility is much smaller in
242 heterozygous as compared to double-mutant *ARID1B* datasets (605 vs. 2140 peaks) (Fig. 2c and
243 Supplementary Fig. 2a), the footprint depth and flanking accessibility analyses produced similar
244 results for both conditions. This somewhat surprising result demonstrates the ability of the
245 footprint depth and flanking accessibility analyses to detect subtle, but highly consistent and likely
246 functional variations in accessibility to TFs that bind in these regions, which otherwise do not
247 exhibit bulk accessibility changes⁵⁶.

248 **ARID1B loss affects distribution of PRC.** Previous studies in both flies and mammals have
249 revealed that BAF opposes PRC to balance genomic accessibility during development^{31,58}. The
250 opposition is produced by direct and dynamic ATP-dependent eviction of PRCs from
251 developmentally repressed loci^{32,33}. Thus, to more clearly understand the mechanism underlying
252 the gene expression changes found in NPCs, we analyzed the localization pattern of H3K27me3
253 and H2AK119ub, the histone modifications produced by PRC2 and PRC1, respectively⁵⁹.
254 Correlational analysis and principal component analysis revealed that genotype was the most
255 significant variable in the samples and that independent biologic replicates were highly correlated
256 (Fig. 4a,b and Supplementary Fig. 3a,b). *ARID1B* heterozygous and double-mutant datasets

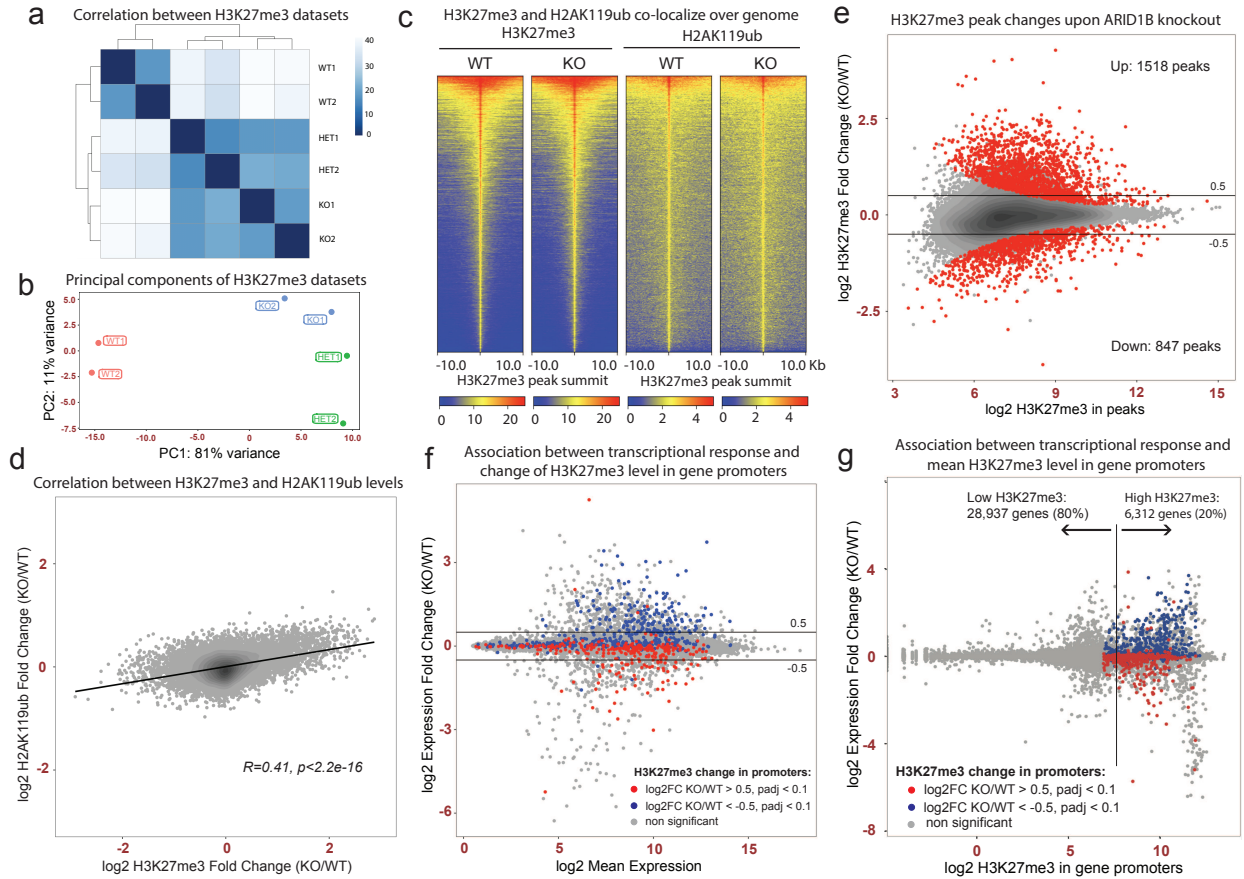


Figure 4: ARID1B dosage sensitive effect on PRC distribution. (a) Correlation between H3K27me3 Cut&Run datasets. (b) Principal component analysis of H3K27me3 Cut&Run datasets. (c) Heatmap displaying H3K27me3 and H2AK119ub distribution around summits of H3K27me3 peaks. (d) Scatter plot displaying log2 fold changes of H3K27me3 versus log2 fold changes of H2AK119ub between KO and WT ARID1B conditions. H3K27me3 and H2AK119ub levels are calculated in ± 3 kb window around H3K27me3 summits. (e) MA plot showing H3K27me3 peak changes between ARID1B WT and KO datasets. Peaks with $|\log 2FC| > 0.5$ and $FDR < 0.05$ are colored in red. (f) MA plot showing gene expression changes between ARID1B WT and KO datasets. Genes with significant changes of H3K27me3 level within ± 3 kb window around their TSS ($|\log 2FC| > 0.5$ and $FDR < 0.1$) are colored in red and blue for increased and decreased H3K27me3 levels respectively. (g) Log2 fold changes of gene expression versus H3K27me3 level within ± 3 kb window around their TSS. Genes with significant changes of H3K27me3 are colored red and blue for increased and decreased H3K27me3 levels respectively. All results are shown for Day 40 after start of hESCs differentiation to NPCs.

258 clustered together away from wild-type, as was seen for gene expression and accessibility. We
 259 found that H3K27me3 and H2AK119ub marks co-localize over the genome as expected from the
 260 coordinated action of PRC1 and PRC2 (Fig. 4c) and exhibit correlated changes across wild-type
 261 and mutant conditions (Fig. 4d). Most of the peaks with significant changes were associated with
 262 increased H3K27me3 level in *ARID1B* double-mutant NPCs (Fig. 4e) consistent with direct ATP-
 263 dependent PRC eviction^{32,33}. GO Biological Process enrichment analysis revealed that decreased
 264 H3K27me3 peaks associate with neural differentiation, confirming our data on enhanced

265 differentiation of *ARID1B* mutant cells (Supplementary Fig. 3c). Specific examples of
266 neurodevelopmental genes that have increased H3K27me3 level in *ARID1B* mutant NPCs include
267 *RBFOX1*, *FOXP2*, *ANK2*, *NR2F1*, and an intron peak within *ARID1B* itself, suggesting that
268 ARID1A might act within a positive feedback loop. (Supplementary Fig. 3d-h). Among those,
269 peaks at *RBFOX1*, *FOXP2* and *NR2F1* also appear in human embryonic stem cells (ESCs), which
270 indicates failure of *ARID1B* mutant NPCs to remove the PRC mark, while peaks at *ANK2* and
271 *ARID1B* appeared *de novo*. Specific examples of neurodevelopmental genes with reduced levels
272 of H3K27me3 in *ARID1B* mutant NPCs include *FOXG1*, *LHX2*, *FZD5*, *OTX1* and *EMX2*
273 (Supplementary Fig. 3i-m).

274

275 **Promoters of differentially expressed genes are associated with high H3K27me3 levels, which**
276 **is not affected by ARID1B loss.** Next, we explored the relationship between changes in
277 H3K27me3 levels within promoter regions (± 3 kb from transcription start sites (TSS)) and gene
278 expression. While we found that genes with decreased (increased) expression are more likely to
279 be associated with increased (decreased) level of H3K27me3 mark (Fig. 4f), the amplitude of
280 H3K27me3 variation was not predictive of gene expression changes. We observed that significant
281 changes in H3K27me3 level in promoters have only minor effects on gene expression levels in
282 most cases. In addition, we found that the majority of the most differentially expressed genes are
283 located in the regions heavily decorated with H3K27me3, which did not exhibit significant
284 changes in *ARID1B* mutant NPCs (Fig. 4g). Indeed, while only 20% of all genes have high
285 H3K27me3 levels within their promoters, they represent 64% of all differentially expressed genes.
286 Of note, the genes with the highest expression changes are associated with the highest level of
287 promoter H3K27me3 that does not change in *ARID1B* mutants. The list of examples of such genes
288 include *EN1*, *EN2*, *CDX2*, *WNT1*, *LMX1A*, *LMX1B*, *RSPO2*, *GDF7*, *DMRT3* (Supplementary Fig.
289 4).

290

291 ***HOX* genes are the most affected by *ARID1B* loss.** In ESCs, *HOX* genes are bivalent and contain
292 histone marks associated with active and repressed chromatin⁶⁰. The bivalent genes are trapped in
293 a state with very low expression until the underlying chromatin is resolved to either fully active or
294 repressed states upon ESC differentiation. Consistent with this paradigm, we observe activation of
295 *HOX* genes upon differentiation of the wild-type ESCs to NPCs. However, *HOX* genes remained
296 silent in the NPCs derived from *ARID1B* heterozygous or double-mutant ESCs (Fig 5a and
297 Supplementary Fig. 5). Activation of the *HOX* genes in the mouse NPCs is accompanied by
298 saltatory and complete clearance of the H3K27me3 histone mark from the underlying genomic
299 loci⁶¹. After 40 days of differentiation, we observed only marginal and statistically insignificant
300 decreases in H3K27me3 marks in the wild-type NPCs as compared to *ARID1B* heterozygous or
301 double-mutant NPCs (Fig. 5b and Supplementary Fig. 5) despite robust differences in Hox gene
302 expression (Fig 5a). To investigate the dynamics of *HOX* genes expression and H3K27me3 marks
303 within the *HOX* loci, we extended our NPC culture for another 20 days and generated RNA-seq
304 and H3K27me3 datasets at day 60 after start of neuronal induction of iPSCs. Analogous to day 40,
305 the expression of *HOX* genes was reduced in *ARID1B* double-mutant NPCs as compared to the
306 wild-type NPCs at day 60 (Fig. 5c). We also observed clearance of H3K27me3 from the underlying
307 genomic loci in the wild-type NPCs but not in the *ARID1B* double-mutant NPCs (Fig. 5d and

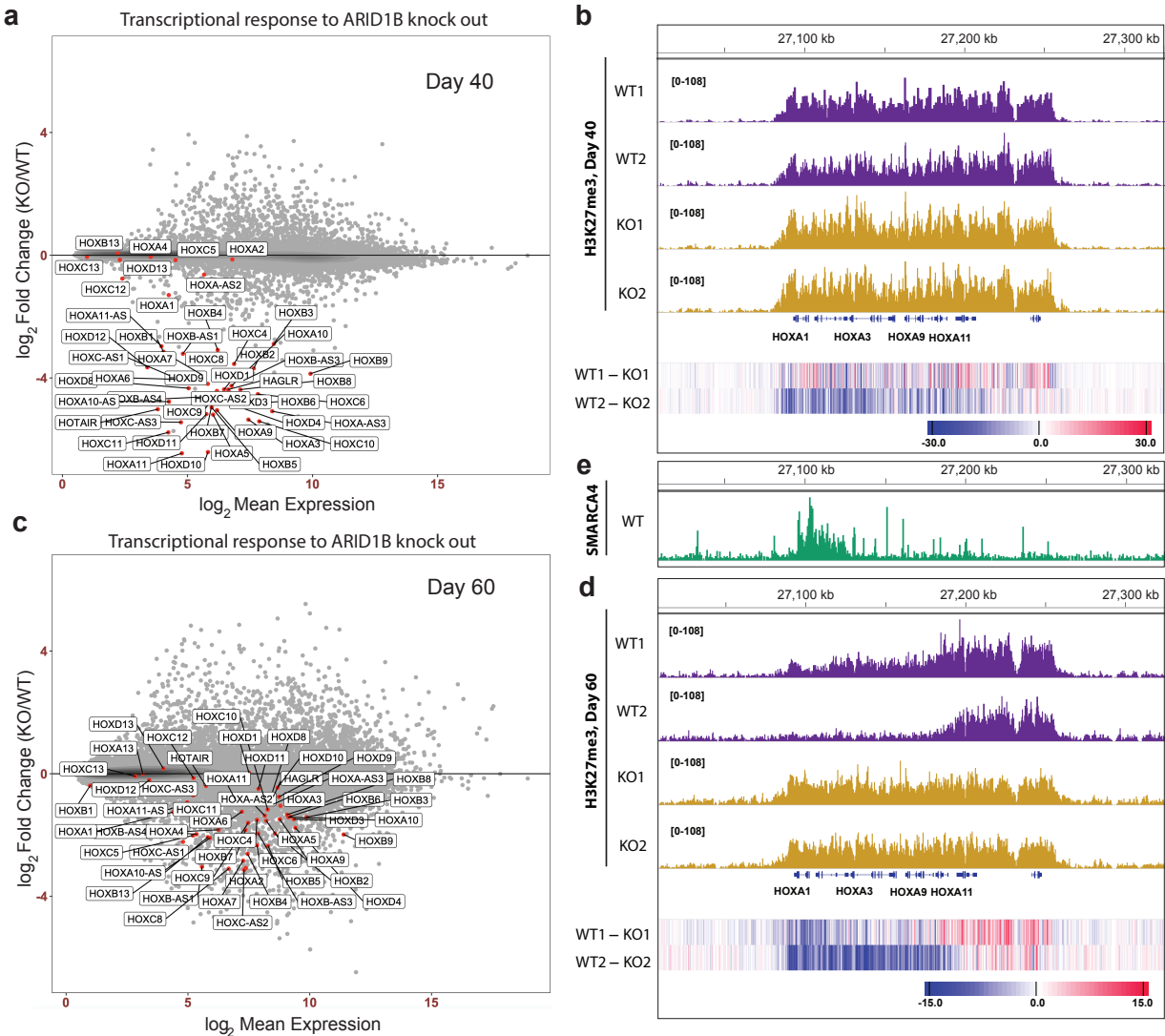


Figure 5: Expression of HOX genes is suppressed in ARID1B mutant NPCs. (a) MA plot showing gene expression changes between ARID1B WT and KO datasets at Day 40 and (c) at Day 60 after start of hESCs differentiation to NPCs. HOX genes and other coding and non-coding genes located within HOX clusters are labeled. (b) H3K27me3 coverage of HOXA locus shown separately for two KO and WT biological replicas at Day 40 and (d) at Day 60. The result of WT and KO subtraction is shown at the bottom of the coverage tracks. (e) SMARCA4 binding within HOXA locus.

308 Supplementary Fig. 6). Surprisingly, these observations suggest that the initial activation of *HOX*
 309 genes occurs prior to H3K27me3 clearance.

310 We observed substantial SMARCA4 presence at all four *HOX* loci in the wild-type NPCs,
 311 with a broad coverage at *HOXA* and *HOXB* domains (Fig. 5e and Supplementary Fig. 5). Together,
 312 our findings suggest that ARID1B is necessary for *HOX* gene activation and for subsequent
 313 heterochromatin resolution to euchromatin.

314

315 **ARID1B mutation affects genes associated with autism spectrum disorders (ASD).** *ARID1B*
 316 and other subunits of BAF complexes are one of the most frequently mutated groups of genes in
 317 ASD⁴⁷. To elucidate functional associations between *ARID1B* and ASD related genes, we
 318 examined our data against the SFARI database, a diverse collection of genes whose *de novo*
 319 mutations are linked to ASD diagnosis. Since most of these mutations are presumably loss-of-
 320 function mutations, we looked for overlap between the SFARI autism genes and genes with
 321 decreased expression in *ARID1B* mutant NPCs. We identified 15 high-confidence ASD genes that
 322 were downregulated ($\log_{2}\text{FC} < -0.5$ and $\text{FDR} < 0.05$) both in heterozygous and double-mutant
 323 *ARID1B* NPCs: *CASZ1*, *NR3C2*, *PAX5* (SFARI score 1), *CGNL1*, *ICA1*, *LMX1B* (SFARI score 2),
 324 and *CDH11*, *EN2*, *ERG*, *MSX2*, *MUC12*, *NXPH1*, *SATB2*, *TNS2*, *WNT1* (SFARI score 3). We also
 325 found that some TFs whose expression is not affected by *ARID1B* mutation nevertheless have
 326 altered flanking accessibility and footprint depth, which suggests defective binding. This group of
 327 TFs include *RFX3*, *SOX5*, *NR4A2*, *MEIS2* (SFARI score 1), *NR2F1*, *NR2F2* (SFARI score 3). In
 328 addition, some high-confidence ASD genes with very low expression in NPCs (e.g.,
 329 *RBFOX1* (SFARI score 2)) have increased
 330 levels of H3K27me3, potentially preventing
 331 their activation later in the course of
 332 development.
 333

334

335 **Enhancing the expression of the**
 336 **endogenous wild-type *ARID1B* allele.**

337 Most neurodevelopmental disorders
 338 associated with *ARID1B* mutations are due to
 339 loss-of-function mutations in one allele. Our
 340 results above indicate that haploinsufficiency
 341 is paralleled by dosage-sensitive changes in
 342 gene expression, accessibility, and PRC
 343 distribution in human NPCs.
 344 Haploinsufficiency is also seen for a large
 345 number of autism genes, indicating that one
 346 might treat these diseases by inducing the
 347 expression of the remaining functional wild-
 348 type allele. For example, some of the autism-
 349 like phenotypes of *Arid1b* mutant mice can be
 350 attributed to deficits in the dorsal raphe of
 351 adult mice and can be rescued with serotonin
 352 analogues⁴⁵. However, genes are subject to
 353 complex positive and negative feedback
 354 pathways that might fix the level of
 355 expression at a stable level. Indeed, *ARID1B* has an intronic regulatory PRC target site sensitive
 356 to the level of the *ARID1B* protein (Supplementary Fig 3e). In addition, studies in yeast have
 357 shown that haploinsufficient genes are often resistant to or intolerant to overexpression⁴⁶. Thus,
 358 we were interested to see if the level of expression from the endogenous gene could be increased
 359 to potentially therapeutic levels, i.e. 2-fold. We employed a rapamycin-inducible FIRE-Cas9
 360 system³⁴ targeted to the *ARID1B* promoter in iPSCs by custom-designed sgRNAs (Fig.

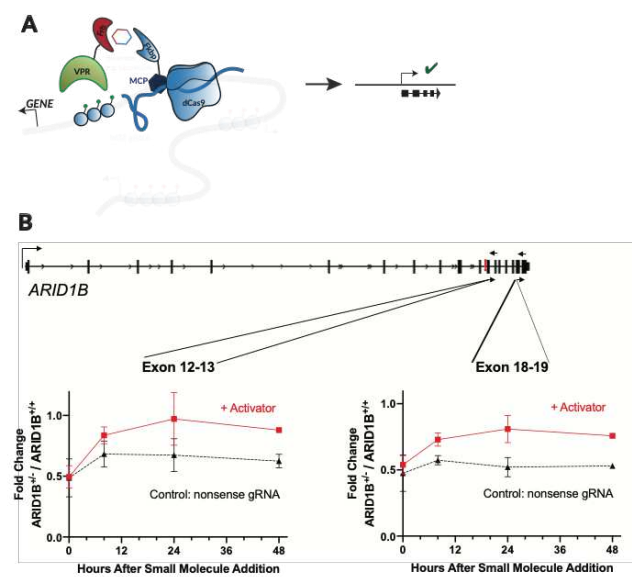


Figure 6: Correction of *ARID1B* expression to the WT level in HET *ARID1B* cell line. (a) Schematic representation of rapamycin inducible FIRE-Cas9 system used to recruit VPR to the *ARID1B* promoter. (b) Time-course of *ARID1B* expression after addition of rapamycin; $n=4$ independent repeats. Two primer sets located at exon 12-13 and exon 18-19 were used for quantifying *ARID1B* expression with qPCR.

Indeed, *ARID1B* has an intronic regulatory PRC target site sensitive to the level of the *ARID1B* protein (Supplementary Fig 3e). In addition, studies in yeast have shown that haploinsufficient genes are often resistant to or intolerant to overexpression⁴⁶. Thus, we were interested to see if the level of expression from the endogenous gene could be increased to potentially therapeutic levels, i.e. 2-fold. We employed a rapamycin-inducible FIRE-Cas9 system³⁴ targeted to the *ARID1B* promoter in iPSCs by custom-designed sgRNAs (Fig.

361 6A). After 24 hours of rapamycin treatment (3 nM), we observed an increase in *ARID1B* mRNA
362 expression to the level comparable to the wild-type (Fig. 6B) as assessed by qPCR using two
363 independent primer sets showing that the full transcript is produced at about 1.8-fold over
364 background (Fig. 6B). Thus, even though *ARID1B* appears to be subject to autoregulation, its
365 mRNA expression can be increased to levels that could be therapeutic using FIRE-Cas9. While
366 the immunogenicity of Cas9 poses a challenge in using the current system as a therapeutic in
367 patients, our proof-of-concept demonstrates the feasibility of activating the endogenous wild-type
368 allele which may be achieved by alternative means such as small molecules.

369
370 **DISCUSSION**
371

372 Our studies show that the haploinsufficient roles that ARID1B plays in human
373 neurodevelopment are paralleled by dosage-sensitive functions in gene expression, genomic
374 accessibility, and distribution of PRC over the genome of human NPCs. Remarkably, ARID1B is
375 required for expression of all four *HOX* clusters. The induction of neural differentiation of human
376 wild type iPSCs is accompanied by increased expression of *HOX* genes and by reduction of the
377 H3K27me3 histone mark from the expressed *HOX* loci. However, *ARID1B*-deficient iPSCs
378 maintain uniform H3K27me3 coverage, characteristic of embryonic stem cells. We find that BAF
379 complexes form broad domains within the *HOX* loci of human NPCs, indicating that clearance of
380 H3K27me3 is likely a result of direct eviction of PRCs by BAF as demonstrated previously^{32,33}.
381 These results parallel classic studies in *Drosophila* which showed that the fly BAP or dSWI/SNF
382 complex maintains expression of homeotic genes during development. Remarkably, the drop in
383 *HOX* gene expression is not only limited to neural progenitors. The analysis of the previously
384 published RNA-seq dataset from the whole brain extract of Arid1b heterozygous male mice
385 revealed that *Hoxb2* is the most downregulated gene ($\log_{2}FC = -8.78$) in the whole dataset with
386 *Hoxd3* exhibiting significant downregulation ($\log_{2}FC = -3.29$)³⁸. Thus, our studies call attention to
387 an evolutionarily conserved pattern played out in the development of the nervous system that
388 underlies the high frequency of human mutations in *ARID1B* and other BAF subunits in human
389 neurodevelopment.

390 Our findings indicate that the mechanism underlying the clearance of Polycomb marks by
391 ARID1B during differentiation of human iPSCs to NPCs appears to result from a complex and
392 temporally specific interplay with critical TFs. Previous work has shown that activation of anterior
393 *Hox* genes (*Hox1-Hox5*) in NPCs is mediated by retinoid acid receptors, which have multiple
394 binding sites within *Hox* loci⁶¹. Remarkably, we showed that in *ARID1B* mutant NPCs, chromatin
395 becomes more inaccessible by ATAC-seq in the vicinity of the binding sites of two retinoic acid
396 receptors RARA and RARG, which suggests that interaction between ARID1B-containing BAF
397 complex and retinoic acid receptors is required for the RA-dependent activation of *HOX* genes.
398 This conclusion is also supported by the evidence of the direct interaction between RARA and
399 ARID1⁶². The activation of posterior *Hox* genes (*Hox6-Hox9*) in the NPCs requires the Cdx2
400 transcription factor binding within *Hox* loci⁶¹. Remarkably, *CDX2* is the most significantly
401 downregulated gene in the *ARID1B*-deficient NPCs in our studies, which could be a consequence
402 of impaired WNT signaling, and downregulation of *WNT3A* as well as several members of the
403 WNT signaling pathway that are required for *CDX2* activation. This observation indicates that
404 *CDX2* may be interacting with BAF, which has the ability to rapidly clear PRC and its marks
405 within minutes^{32,33}. Consistent with this mechanism, *CDX2* was previously shown to directly
406 interact with the BAF complex^{63,64}. Thus, our studies and those previously reported indicate that

407 ARID1B-containing BAF complexes act early in iPSC-to-NPC differentiation by first cooperating
408 with retinoid acid receptors localized to the *HOX* loci. A second mechanism used by ARID1B is
409 to contribute substantially to the activation of *CDX2*, whose gene product appears to guide BAF
410 to the *HOX* loci, which then rapidly and directly evict PRC in an ATP-dependent fashion^{32,33}.

411 The BAF complex counteracts repression mediated by PRC1 and PRC2. Indeed, we
412 observe robust changes in H3K27me3 distribution in *ARID1B* deficient NPCs. We also found that
413 increase (decrease) in gene expression was associated with decreased (increased) H3K27me3 level
414 in gene promoters. However, the amplitude of H3K27me3 changes within gene promoters was not
415 predictive of the amplitude of transcriptional changes. Remarkably, we found that the genes
416 exhibiting the largest changes in transcription have high H3K27me3 level that does not change in
417 *ARID1B* mutants, which indicates that regulation of transcription by PRC is a more complicated
418 process than simple changes in H3K27me3 levels⁶⁵. These findings indicate that in mammals,
419 BAF complexes use additional mechanisms to control critical developmental genes, such as
420 nucleosome remodeling, regulation of histone acetylation by interaction with CBP⁶⁶⁻⁶⁸, and
421 regulation of chromosomal topology with Topoisomerase 2²⁵.

422 We also find that ARID1B has programmatic roles in regulating both the expression and
423 function of WNT and TGF- β signaling pathways. During the course of iPSC-to-NPC
424 differentiation, ARID1B directly regulates many genes required for these signaling pathways
425 leading to well characterized phenotypes that might be related to the neurodevelopmental
426 abnormalities found in individuals having mutations in one allele of *ARID1B*. In addition to the
427 regulation of *HOX* genes, we also found programmatic roles in controlling the accessibility of
428 binding sites of SOX family of transcription factors and multiple nuclear receptors important in
429 human neurodevelopment. *ARID1B* is a high confidence autism gene and we observe that several
430 genes previously associated with ASD have decreased expression in *ARID1B* heterozygous and
431 double-mutant NPCs. In addition, several TFs associated with ASD have altered accessibility
432 profiles in *ARID1B* mutant NPCs indicating their deficient binding and function.

433 BAF complexes are combinatorially assembled with 15 to 17 subunits encoded by 29 to 31
434 genes⁶⁹⁻⁷³. Based on immunofluorescence studies and single cell RNA sequencing it appears that
435 each cell contains perhaps 100 or more distinct complexes⁷⁴, raising the issue of how functionally
436 diverse or redundant these complexes might be. Remarkably, while the *ARID1B* expression level
437 is only about 30% of *ARID1A* expression in our samples, ARID1A cannot compensate for
438 ARID1B deletion, which indicates unique roles for ARID1B-containing complexes. ARID1A-
439 containing complexes have a dramatically different function in the nervous system⁷⁵. The unique
440 and non-redundant functionality of different combinatorially assembled BAF complexes is further
441 supported by the fact that both *ARID1A* and *ARID1B* are haploinsufficient and dosage-sensitive in
442 the nervous system. The molecular mechanism by which these homologous proteins play such
443 different functions is not yet clear, but localization, differential TF interactions and perhaps
444 different roles in nucleosome dynamics or PRC opposition are all possibilities.

445 Based on recent sequencing studies, it appears that *de novo* loss of function mutations in
446 haploinsufficient genes are common causes of human disease. These diseases might be treated by
447 boosting transcription of the functional endogenous allele to overcome the reduction of the normal
448 gene product due to the defective allele. Concomitant increase in the expression of the defective
449 allele should not be an obstacle for this strategy as long as the defective allele is not a dominant
450 negative. However, Amon and colleagues have found that in yeast, haploinsufficiency is often
451 accompanied by intolerance or resistance to overexpression⁴⁶, which would foil this simple
452 therapeutic strategy. In addition, many genes including *ARID1B* appear to operate within powerful

feedback pathways that could make a cell resistant to altering the level of expression of an endogenous gene. To test this possibility for the remarkably dosage-sensitive ARID1B gene, we used FIRE-Cas9 to conditionally activate the expression of *ARID1B*. Remarkably, in heterozygous *ARID1B* iPSCs, 3 nM rapamycin activated transcription along the entire 400 kb gene to a stable level of expression about 1.8-fold above that found in the mutant cells. While the immunogenicity of Cas9 makes the system unsuitable for clinical studies, these preliminary experiments suggest that no intrinsic barrier exists to limit expression of *ARID1B* mRNA and that perhaps a small molecule could specifically induce expression of this gene, much in the same way that topotecan unsilences the paternally encoded Ube3a in Angelman syndrome⁷⁶. Furthermore, we have recently found that ARID1B executes its social functions in neurons of the dorsal raphe of the adult mouse⁴⁵ indicating that this strategy could evolve into an effective treatment.

465 METHODS

467 Generation of *ARID1B* isogenic iPSC lines

468 Human iPSCs derived from an *ARID1B*-heterozygous Coffin-Siris patient (*ARID1B* c.2598del)
 469 were a generous gift from the Santen laboratory (Leiden University). The iPSCs were cultured in
 470 mTeSR1 medium (Stemcell Tech.) on plates coated with Geltrex (ThermoFisher) and passaged
 471 with Accutase (Stemcell Tech.) every 4-5 days. Genome editing was performed using the protocol
 472 described in Ran FA, HsuPD, Wright J, Agarwala V, Scott DA, Zhang F. Nat Protoc 2013;
 473 8(11):2281-308 (PMID 24157548). A brief protocol is as follows. **Molecular cloning.** Single-
 474 guide RNAs (sgRNAs) sequences targeting exon 9 of the human *ARID1B* gene were designed
 475 using the tool developed in the Zhang lab (crispr.mit.edu) and cloned into the pSpCas9-2A-puro
 476 (Addgene, catalog no. 48139). The following sgRNA was chosen for the experiments following
 477 optimization: 5'-CTGGGCACCCCACTATACGC. HDR (homology directed repair) templates
 478 were generated by inserting into pUC19 either the wild-type (5'-
 479 agctctcctgctgccgtgccgtctgtctggacagtttccgagatgtggcagccagcacaaccagctgcgtcgatctgttactcaag
 480 caaaaaaaaaaaaaagaaaaagaaaaatatttccaaacttagaggaaaactggggctcatgtcaggtcccgctgacacccctgttgcgg
 481 ggtttaaaggatgatttgaccatatgtcatgtcgcttacacgttgcgtttgagcccttcacatgactgttgaaggtagcagtgtatctgt
 482 gtgtgtatctaagagtgtgtcaccatttgttaaaatataagaatatgtgtgttgaatggattgaggcagcactcggtgtccctgttgcctt
 483 catagggttgcgtttttgtttttgtttgttgcattttatgaccagcctgaatttcctcatcagtcagtgccgttgcgttgcgttgcgttgcctt
 484 ctctctgaggccctgggagtgtgcagagagagcatgttgcagactggcagctgcaccaggcagcaacaggaaaggccataacggcatt
 485 actaatactccgtgtatgcatt
 486 ttaggttaactactccaggccctccaggctatgtgggtgcccaggctgcaagCtacagccggccaggccggatgggtatgggtatcgtgc
 487 caaccaggatgtggacaaggccaaggccaggccatgtggctgtgcctggacgaatgccatcagctggatgcagaacagacc
 488 atttcctggaaatatgagcagcatgacccttcaggatgttgcgttgcgttgcgttgcgttgcgttgcgttgcgttgcgttgcgttgc
 489 aaccgtaaaggcacaggaggcagccgcagcagtgtatgcaggctgtcgactcagcacaaggatgggtatgggtatgggtatgggtatgg
 490 ccggccaggatgtggctgtgttgcgttgcgttgcgttgcgttgcgttgcgttgcgttgcgttgcgttgcgttgcgttgcgttgcgttgc
 491 actgtgttgcgttgcgttgcgttgcgttgcgttgcgttgcgttgcgttgcgttgcgttgcgttgcgttgcgttgcgttgcgttgcgttgc
 492 aatgtgttgcgttgcgttgcgttgcgttgcgttgcgttgcgttgcgttgcgttgcgttgcgttgcgttgcgttgcgttgcgttgcgttgc
 493 gaagtgtgttgcgttgcgttgcgttgcgttgcgttgcgttgcgttgcgttgcgttgcgttgcgttgcgttgcgttgcgttgcgttgcgttgc
 494 actccccaccccttccaccacaagaatcttctaaaatacaacttcgtatgtatcgttgcgttgcgttgcgttgcgttgcgttgcgttgc
 495 tgagatattatacttgcatt
 496 or mutant (5'-
 497 agctctcctgctgccgtgccgtctgtctggacagtttccgagatgtggcagccagcacaaccagctgcgtcgatctgttactcaag
 498 caaaaaaaaaaaaaagaaaaagaaaaatatttccaaacttagaggaaaactggggctcatgtcaggtcccgctgacacccctgttgcgg
 499 ggtttaaaggatgatttgaccatatgtcatgtcgcttacacgttgcgttttgcgttgcgttgcgttgcgttgcgttgcgttgcgttgcgttgc

499 gtgtatctaagagtgtgtcaccatttggtaaaatataagaatatgggtgtgaatgggattgaggcagcactcggtgtccctgccttat
 500 catagggttgttttgttttgttctttatgaccagcctgaattcttcattcatcagtgcagtggcctctgggctgtctgtatggactca
 501 ctctctgagggcctggagtgtagcagagagagcatgttgagactggcagctgcaccagcagcaacaggaaggccctataacggctatg
 502 actaatactccgtgtatgcattgtggacaaaagtattccactgtgaatgtgtcacaagttaaataaaaggcttactttgtttgtttttgt
 503 ttaggttaactactccaggcctccagcgtatgtgggtgcccagtgcagatcagcggcccagggcccgtatgggtatcagtgcaccaaca
 504 accagatgcatggacaaggccaaagccagccatgt
 505 cctggaaatatgagcagcatgacccccagttctcctggcatgtctcagcagggagggcaggaatggggcccaatgcacactgtgaac
 506 cgttaaggcacaggaggcagccgeagcagtgatgcaggctgtgcgaactcagcacaaggcaggtagcacccaggagcacgcccc
 507 gggcaggtacgtgtgtctaccctgtgaccacgtactgcgcacatagctgtgtgtgtgtgtgtgtgtgtgtgtgtgtgtgtgtgt
 508 gt
 509 gtgagcggtgagcacatcagtcgtggaggtgatggaaatgcctgtgaatagtcattgcagcagcacaaccagatctgggtcacaggaa
 510 gtgtctgcgt
 511 cccacccatcc
 512 gatttataacttgacattttatgttatccaggcatatctgtccaaacca) *ARID1B* gene sequence via the BamHI site; note that a new silent restriction site was incorporated into the HDR templates (5'-
 513 aggccct from the native sequence 5'-agacc). **Transfection.** Human pluripotent stem cells were
 514 grown in mTeSR1 medium (Stem Cell Technologies) on plates coated with Geltrex (Invitrogen).
 515 At ~70% confluence, cells were dissociated to near single cells using Accutase (Life
 516 Technologies). 10⁶ cells were transfected with 5 ug total DNA (1:1 w/w mixture of pSpCas9-
 517 sgRNA with or without HDR repair template) using Amexa Human Stem Cell NucleofectorTM Kit
 518 1 (Lonza) according to the manufacturer's protocol. **Drug selection, genotyping, and qRT-PCR.**
 519 At 24h post-transfection, puromycin (0.5-0.75 ug/ml) was added to culture medium for 48h.
 520 Individual colonies were manually picked after 7-10 days and expanded. Genomic DNA for each
 521 clone was prepared by incubating cells overnight at 55°C in 0.1 mg/ml proteinase K in digestion
 522 buffer (100 mM NaCl, 10 mM TrisCl pH 8, 25 mM EDTA pH 8, 0.5% SDS) followed by heat
 523 inactivation at 85°C for 10 minutes. The target region in *ARID1B* was amplified by PCR (Fw
 524 primer: 5'- ctggggctgtgtatggactctc; Rv primer: 5'-aaatgagtaatgttagctaaaggccctt) and
 525 sequenced using the following primer: 5'-atccctggccctccctgtgagacatg.
 526

Quantitative real-time polymerase chain reaction (qRT-PCR)

The *ARID1B* isogenic iPSC lines with the desired genotypes (wild-type, heterozygous, or double mutant) were verified by analyzing *ARID1B* mRNA transcription by qRT-PCR. Briefly, total RNA was isolated using TRIzol™ Reagent (Thermo Fisher) and cDNAs were synthesized using SuperScript™ Double-Stranded cDNA Synthesis Kit (Thermo Fisher) following the manufacturer's instructions. qRT-PCR was performed in QuantStudio 6 Flex Real-Time PCR System (Thermo Fisher) with SensiFAST™ SYBR Lo-ROX Kit (Bioline) using primer sets targeting exons 12-13 (Fw: 5'-CTACGTCTGCGTCAAAGAGATCG; Rv: 5'-GTTGCCAGCTCACGCCACTTCTTG) or exons 18-19 (Fw: 5'-GCATCACACCAGTCTGAAACAA; Rv: 5'-ATCACACGCCACGCCTCAGGAGTA) of the *ARID1B* gene. *GAPDH* was used as a control gene (Fw: 5'-GGTGGTCTCCTCTGACTTCAA C; Rv: 5'-TTCGTTGTCATACCAGGAAATG).

Human Pluripotent Stem Cell Differentiation into the Neural Lineage

542 Human iPSC cultures were maintained in mTeSR1 medium (StemCell Technologies). To start
543 NPC differentiation, cells were dissociated to single cells using Accutase (Life Technologies) and
544 re-aggregated for 48h in Ultra-Low Cluster 96-well round bottom plates (CoStar) at a density of

545 7500 cells per well in mTeST1 supplemented with 1 uM Thiazovivin. On day 1 of differentiation,
546 an equal volume of Neural Induction Medium (NIM) was added: 10% Knock-Out Serum
547 Replacement, Penicillin/Streptomycin, and GlutaMax in Dulbecco's Modified Eagle Medium
548 (DMEM) (Life Technologies) supplemented with 10 uM RepSox (Tocris), 1 uM LDN-193189
549 (StemCell Technologies), and 1 uM Thiazovivin. From day 2 to day 5, half of the spent medium
550 was removed daily and replaced with fresh NIM without Thiazovivin. Starting on day 6, Neural
551 Progenitor Medium (NPM) was used, containing 2% B27 Supplement without vitamin A,
552 Penicillin/Streptomycin, and GlutaMax in DMEM/F12 (Life Technologies) supplemented with 20
553 ng/ml EGF and 20 ng/ml FGF (PeproTech); 10 uM RepSox was only added until day 10. On day
554 7, cell aggregates were transferred to Geltrex (Life-Technologies)-coated 6-well plates. Neural
555 rosettes were carefully dissected from the adherent culture on days 12-14 and maintained as
556 neurospheres in suspension, with medium change every 1-2 days and gentle dissociation by
557 trituration every 4-5 days until the cells were used in experiments. EGF and FGF were omitted
558 from the NPM medium starting on day 40.

559
560

561 FIRE-Cas9 Rapid and Inducible Activation of *ARID1B*

562 Activation of *ARID1B* in human iPSC *ARID1B*^{+/−} cultures were carried out in four independent
563 experiments using the FIRE-Cas9 activation (VPR) system described in³⁴. Briefly, iPSC cultures
564 were sequentially infected with lentiviral constructs and selected using an appropriate antibiotic
565 (blasticidin: 5ug/mL; hygromycin: 25ug/mL, puromycin: 0.75ug/mL, zeocin: 25ug/mL).
566 Throughout, infection and selection concentrations were carefully titred and cultures were
567 monitored for maintenance of pluripotency with microscopy. 3nM rapamycin was added for 8-48
568 hrs to induce activation. Cultures were washed 1X with ice-cold PBS and total RNA was extracted
569 with Trisure (Bioline), purified, and DNase-treated using the Direct-zol RNA kit (Zymo). cDNA
570 was synthesized from 1 ug RNA using the SensiFAST kit (Bioline). For RT-qPCR, samples were
571 prepared using the SYBR LO-ROX kit (Bioline) and analyzed on a QuantStudio 6 Flex (Life
572 Technologies). Two sets of *ARID1B* primers targeting two different exons were chosen based on
573 a standard curve analysis and Ct values were normalized to Ct values for the housekeeping gene
574 *GAPDH* (dCt = Ct_{*ARID1B*} − Ct_{*GAPDH*}) for each sample before further analysis. Primer sequences are:

575 *ARID1B* Exon12-13 fwd: CTACGTCTCGTCAAAGAGATCG
576 *ARID1B* Exon12-13 rev: GTTGCCAGCTCACGCCACTTCTTG
577 *ARID1B* Exon18-19 fwd: GCATCACACCAGTCTGAAACAA
578 *ARID1B* Exon18-19 rev: ATCACACGCCACGCCCTCAGGAGTA
579 *GAPDH* fwd: GGTGGTCTCCTCTGACTTCAAC
580 *GAPDH* rev: TTCGTTGTCATACCAGGAAATG

581 Guide Design: spCas9 guide RNAs (gRNAs) targeting the *ARID1B* promoter were designed using
582 the GPP sgRNA Design Tool/CRISPRick^{77,78} and cloned into lentiviral constructs (Lv U6 sgRNA-
583 2xMS2-sgRNA EF1 Zeo) from³⁴. sgRNA sequence: CCGCGCGGCCATGATCGCCG

584 Lentivirus Production: HEK293T cells were transfected with 18ug of the respective lentiviral
585 construct (Lv U6 sgRNA-2xMS2-sgRNA EF1 Zeo, Lv EF1a dCas9-2A-Blast, Lv EF1a MCP-
586 2xFkb-2A-Hygro, Lv EF1a VPR-2xFrb Pkg Puro; described in³⁴ and packaging plasmids
587 (psPAX2 and pMD2.G) using PEI (Polysciences). 48hrs after transfection, the media was
588 collected, filtered with a 0.45 um filter (Millipore), and ultra-centrifuged at 50,000 x g for 2hrs at
589 4°C. The viral pellet was resuspended in PBS and used for infection.

590

591 **RNA-seq Library Preparation**
592 Cultures were washed 1X with ice-cold PBS and total RNA was extracted with Trisure (Bioline),
593 purified and DNase-treated using the Direct-zol RNA kit (Zymo). Libraries were prepared from
594 500ng RNA with dual-index unique barcodes using the SMARTer Stranded Total RNA Sample
595 Prep HI Kit (Clontech), quantified by qPCR using a PhiX (Illumina) standard curve, and checked
596 for appropriate fragment size distribution by Tapestation (Agilent). Libraries were pooled and
597 multiplexed 1:1 and run on a HiSeq3000 (Illumina) for 2x150 paired-end sequencing (Novogene)
598 with a 20% PhiX spike-in.
599

600 **ATAC-seq library preparation**

601 Cells were washed and collected in ice-cold PBS using a cell lifter (Corning #3008), and then
602 counted using a Countess II FL cell counter (Applied Biosystems). Accessible chromatin from
603 75,000 cells per biological sample were transposed and tagged using Tn5 (Nextera DNA Sample
604 Prep Kit from Illumina, cat# FC-121-1030), then barcoded and amplified following a published
605 protocol (PMID: 24097267). DNA fragment sizes were determined using a TapeStation (Agilent)
606 with High Sensitivity D1000 ScreenTapes (Agilent cat# 5067-5584) and showed the expected
607 pattern for non-nucleosomal and nucleosomal sizes. Libraries were quantified by PCR using a
608 PhiX library (Illumina cat# TG-110-3001) standard curve and then multiplexed at a 1:1 ratio.
609 Pooled libraries were run on a HiSeq3000 (Illumina) for 2x75 paired-end sequencing at the
610 Stanford Functional Genomics Facility.
611

612 **CUT&RUN Sample Preparation**

613 Cultures were washed 1X with ice-cold PBS and dissociated to single cells using Accutase (Life
614 Technologies). CUT&RUN was performed with an anti-H3K27me3 antibody (ActiveMotif rabbit
615 polyclonal #39155) as described in ⁷⁹. Briefly, exactly 250,000 cells were counted with an
616 automated cell counter (Countess, Life Technologies), bound to Concanavalin A beads
617 (BioMagPlus, Bangs Laboratories #BP531). The anti-H3K27me3 antibody was added (1:50
618 dilution) and incubated with cells under 800rpm shaking at 4°C for 2 hrs. After wash steps, a 1:200
619 dilution of proteinA-MNase was added and incubated for 1hr at 4°C. After washing, 100mM CaCl₂
620 was added at 0°C and incubated for 15 mins to activate the MNase. The reaction was stopped by
621 addition of a 10mM EDTA/EGTA Stop Buffer (see Meers et al. 2019 for details), incubated at
622 37°C for 10mins, and centrifuged at 4°C, 5000xg for 15 mins. The supernatant containing DNA
623 was taken and purified with the DNA Clean and Concentrator Kit (Zymo). Samples were
624 quantified on a HS DNA Qubit Fluorometer (Life Technologies) and fragment size distribution
625 checked with a Tapestation (Agilent).
626

627 **CUT&RUN Library Preparation**

628 Dual-index libraries were prepared from CUT&RUN eluted DNA using the NEBNext Ultra II
629 DNA Library Prep (E7103S) with NEBNext Multiplex Oligos for Illumina (Dual Index Primers
630 Set 1, E7600S) following manufacturer instructions. Libraries were quantified by qPCR using a
631 PhiX (Illumina) standard curve, and checked for appropriate fragment size distribution by
632 Tapestation (Agilent). Libraries were pooled and multiplexed 1:1 and run on a HiSeq3000
633 (Illumina) for 2x150 paired-end sequencing (Novogene).
634

635 **RNA-seq data analysis**

636 Raw reads were pseudoaligned to GENCODE v33 human transcriptome assembly⁸⁰ and transcript
637 abundance was quantified using kallisto (version 0.44.0)⁸¹. Transcript abundance files from
638 kallisto output were imported to R using tximport⁸². DESeq2⁸³ was used for analysis of
639 differential gene expression. For visualization and gene ranking we used effect size shrinkage for
640 Log2FC estimates as encoded by *ashr()* function⁸⁴. Enrichr⁸⁵ was used for GO-term analysis of
641 differentially expressed genes, defined as genes with $|\log_{2}FC| > 0.5$ and $FDR < 0.05$. PANTHER
642 Pathway analysis was performed using PANTHER⁸⁶.

643

644 **ATAC-seq data analysis**

645 The adapters were trimmed from the raw reads using *trim_galore* and *cutadapt*⁸⁷. The trimmed
646 reads were aligned to GRCh38 human genome assembly using bowtie2⁸⁸ with *--very-sensitive -X2000*
647 parameters. Not aligned reads and paired reads with at least one read in a pair falling below
648 quality score threshold 10 were removed using *samtools*⁸⁹ and *awk* text editor. Additionally,
649 paired reads were removed if each read in a pair have multiple alignment sites. PCR and optical
650 duplicates were removed using *Picard*. Tn5 insertion sites were defined as the start read position
651 offset by +4 bp for the reads aligned to + strand and as the end read position offset by -5 bp for the
652 reads aligned to - strand⁹⁰. Macs2 (v2.1.1)⁹¹ was used to reconstruct accessibility peaks around
653 Tn5 insertion sites with the following parameters *--shift -75 --extsize 150 --nomodel --call-summits*
654 *--nolambda --keep-dup all -p 0.01*. To derive consensus peak set we (1) merged individual
655 biological replica data sets across each condition (WT, HET, KO), (2) applied *macs2* on the
656 merged data sets and filtered out all peaks falling below the random quality threshold 100, (3)
657 merged resulting peaks using *bedtools*⁹². The raw counts in the peak regions were calculated using
658 *bedtools*. Peak differential analysis was performed using DESeq2⁸³. GO-term enrichment analysis
659 was performed using GREAT web server⁹³ on a set of peaks with differential accessibility, with
660 a set of all accessibility peaks used as a background. HOMER⁹⁴ was used to perform TF
661 enrichment analysis in the differentially accessible peaks, defined as peaks with $|\log_{2}FC| > 0.5$ and
662 $FDR < 0.05$. A heatmap was produced using deeptools (version 3.3.0)⁹⁵.

663

664 **Footprint Depth and Flanking accessibility analysis**

665 We used non-redundant position frequency matrices from JASPAR 2020⁹⁶ CORE (vertebrates)
666 and UNVALIDATED collections comprising 746 and 337 transcription factors respectively.
667 FIMO tool from the MEME Suite⁹⁷ was used to locate individual transcription factor binding sites.
668 The sites with identical genomic coordinates located on the opposite strands were merged. For
669 each TF within each individual ATAC-seq dataset we built an accessibility profile, defined as the
670 number of Tn5 insertion sites counted as function of distance from the TF motif borders. The
671 counting was done over all TF motifs present within accessibility peaks. Based on TF accessibility
672 profiles we defined Flanking Accessibility (FA) and Footprint Depth (FPD).

673
$$FA = \sum_i \log_2 \frac{\bar{N}_{FLANK}}{\bar{N}_{BG}}$$

674 where \bar{N}_{FLANK} is a number of Tn5 insertion sites found in the region adjacent to TF motif, [-55 bp,
675 -6 bp] U [6 bp, 55 bp], and divided by the region length. - and + refer to nucleotides located
676 upstream and downstream the lower and upper motif boundaries respectively. \bar{N}_{BG} is a number of
677 Tn5 insertion sites in the background region, [-250 bp, -200 bp] U [200 bp, 250 bp], divided by
678 the region length. The index i runs over all biological replicas in a single condition (KO, HET,
679 WT).

$$680 \quad FPD = \sum_i \log_2 \frac{\bar{N}_{MOTIF}}{\bar{N}_{FLANK}}$$

681 where \bar{N}_{MOTIF} is a number of Tn5 insertion sites in the region centered on the motif, [-5 bp, 5 bp],
 682 divided by the region length. To evaluate changes in TF binding across conditions, we calculated
 683 $\Delta FA_{TF} = FA^{KO(HET)} - FA^{WT}$ and $\Delta FPD_{TF} = FPD^{KO(HET)} - FPD^{WT}$. A statistical significance
 684 (p-value) of $(\Delta FA, \Delta FPD)_{TF}$ was evaluated using bootstrapping technique as follows. For each TF
 685 and each condition (KO, HET, WT), we built an artificial accessibility profile from a set of motifs
 686 randomly selected from a set we used for $(\Delta FA, \Delta FPD)_{TF}$ calculations. A single motif could be
 687 selected multiple times. The total number of selected motifs was equal to the size of the motif set
 688 used for $(\Delta FA, \Delta FPD)_{TF}$ calculations. For each selected motif Tn5 insertion sites from a randomly
 689 chosen biological replica within a single condition were merged into the artificial accessibility
 690 profile. These artificial accessibility profiles were used to calculate new ΔFA and ΔFPD values.
 691 The procedure was repeated 10,000 times resulting in a bootstrapped $(\Delta FA, \Delta FPD)$ distribution
 692 built separately for each TF, which reflects the statistical uncertainty in evaluation of ΔFA and
 693 ΔFPD for that TF. To evaluate p-value, we created a 1-dimensional histogram, filled with the
 694 number of $(\Delta FA, \Delta FPD)$ points found within bins along the axis connecting a center of
 695 bootstrapped $(\Delta FA, \Delta FPD)$ distribution and $(\Delta FA, \Delta FPD)_{TF}$ observed for specific TF. FDRs
 696 were calculated using Benjamini & Hochberg correction for multiple comparisons using R `p.adjust`
 697 function. For visualization purpose we placed the center of $(\Delta FA, \Delta FPD)$ distribution into the
 698 origin of the coordinate system and labeled TFs, with FDR less than 0.05 and random threshold
 699 on minimal expression at 50 normalized counts.
 700

701 **CUT&RUN H3K27me3 data analysis**

702 The adapters were trimmed from the raw reads using *trim_galore* and *cutadapt*⁸⁷. The trimmed
 703 reads were aligned to GRCh38 human genome assembly using bowtie2⁸⁸ with *--very-sensitive -X2000*
 704 parameters. Not aligned reads and paired reads with at least one read in a pair falling below
 705 quality score threshold 10 were removed using *samtools*⁸⁹ and *awk* text editor. Additionally,
 706 paired reads were removed if each read in a pair have multiple alignment sites. PCR and optical
 707 duplicates were removed using *Picard*. *Macs2* (v2.1.1)⁹¹ was used to reconstruct peaks from
 708 fragments with the following parameters *--format BEDPE -B --call-summits --nolambda -p 0.01*.
 709 To derive consensus peak set we (1) merged individual biological replica data sets across each
 710 condition (WT, HET, KO), (2) applied *macs2* on the merged data sets and filtered out all peaks
 711 falling below the random quality threshold 200, (3) merged resulting peaks using *bedtools*⁹². The
 712 raw counts in the peak regions were calculated using *bedtools*. Peak differential analysis was
 713 performed using DESeq2⁸³. GO-term enrichment analysis was performed using GREAT web
 714 server⁹³ on a set of peaks with significant change in H3K27me3 level across conditions. A
 715 significant change was defined as $|\log_2 FC| > 0.5$ and $FDR < 0.05$. A set of all peaks was used as a
 716 background.
 717

718 **Cut&Run H2AK119ub data analysis**

719 The adapters were trimmed from the raw reads using *trim_galore* and *cutadapt*⁸⁷. The trimmed
 720 reads were aligned to GRCh38 human genome assembly using bowtie2⁸⁸ with *--very-sensitive -X2000*
 721 parameters. Not aligned reads and paired reads with at least one read in a pair falling below
 722 quality score threshold 10 were removed using *samtools*⁸⁹ and *awk* text editor. Additionally,
 723 paired reads were removed if each read in a pair have multiple alignment sites. PCR and optical

724 duplicates were removed using *Picard*. Macs2 (v2.1.1) ⁹¹ was used to reconstruct peaks from
725 fragments with the following parameters --format BEDPE -B --call-summits --nolambda -p 0.01.
726

727 **Analysis of autism related genes**

728 We used SFARI gene database of autism related genes (release 1/13/2021).

729 **Acknowledgements**

730 We thank members of the Crabtree lab for their comments and discussions. We are grateful to
731 Chris Weber for providing critical comments on the manuscript and fruitful discussions. This study
732 was supported by Walter V. and Idun Berry Foundation, Howard Hughes Medical Institute,
733 Stanford MedScholars Fellowship.

734 **Author Contributions**

735 E.Y.S. and A.K. conceived the project. E.Y.S. derived the cell lines and performed RNA-seq and
736 ATAC-seq experiments. E.Y.S. and S.G. designed and performed the *ARID1B* activation
737 experiment. E.Y.S., A.K. and C.Y.C. performed the CUT&RUN experiments. A.K. performed
738 data analysis. A.K., E.Y.S., and G.R.C. wrote the manuscript with contribution from all authors.
739 G.R.C. designed experiments and supervised the project.

740 **Competing interests**

741 G.R.C. is founder and stockholder of Foghorn Therapeutics. The other authors declare no
742 competing interests.

743 **REFERENCES**

1. Abrams, E., Neigeborn, L. & Carlson, M. Molecular analysis of SNF2 and SNF5, genes required for expression of glucose-repressible genes in *Saccharomyces cerevisiae*. *Mol. Cell. Biol.* **6**, 3643–3651 (1986).
2. Stern, M., Jensen, R. & Herskowitz, I. Five SWI genes are required for expression of the HO gene in yeast. *J. Mol. Biol.* **178**, 853–868 (1984).
3. Tamkun, J. W. *et al.* brahma: A regulator of *Drosophila* homeotic genes structurally related to the yeast transcriptional activator SNF2 SWI2. *Cell* **68**, 561–572 (1992).
4. Lessard, J. *et al.* An Essential Switch in Subunit Composition of a Chromatin Remodeling Complex during Neural Development. *Neuron* **55**, 201–215 (2007).
5. Wu, J. I. *et al.* Regulation of Dendritic Development by Neuron-Specific Chromatin Remodeling Complexes. *Neuron* **56**, 94–108 (2007).
6. Yoo, A. S., Staahl, B. T., Chen, L. & Crabtree, G. R. MicroRNA-mediated switching of chromatin-remodelling complexes in neural development. *Nature* **460**, 642–646 (2009).
7. Yoo, A. S. *et al.* MicroRNA-mediated conversion of human fibroblasts to neurons. 3–7 (2011). doi:10.1038/nature10323
8. Braun, S. M. G. *et al.* BAF subunit switching regulates chromatin accessibility to control cell cycle exit in the developing mammalian cortex. *Genes Dev.* **35**, 335–353 (2021).
9. Son, E. Y. & Crabtree, G. R. The role of BAF (mSWI/SNF) complexes in mammalian neural development. *Am. J. Med. Genet. Part C Semin. Med. Genet.* **166**, 333–349 (2014).
10. van der Sluijs, P. J. *et al.* The ARID1B spectrum in 143 patients: from nonsyndromic intellectual disability to Coffin–Siris syndrome. *Genet. Med.* **21**, 1295–1307 (2019).

- 770 11. Koshio, T., Miyake, N. & Carey, J. C. Coffin-Siris syndrome and related disorders
771 involving components of the BAF (mSWI/SNF) complex: Historical review and recent
772 advances using next generation sequencing. *Am. J. Med. Genet. Part C Semin. Med.*
773 *Genet.* **166**, 241–251 (2014).
- 774 12. Cheng, S. S. W., Luk, H. M., Mok, M. T. S., Leung, S. S. & Lo, I. F. M. Genotype and
775 phenotype in 18 Chinese patients with Coffin-Siris syndrome. *Am. J. Med. Genet. Part A*
776 (2021). doi:10.1002/ajmg.a.62187
- 777 13. Santen, G. W. E. *et al.* The ARID1B phenotype: What we have learned so far. *Am. J. Med.*
778 *Genet. Part C Semin. Med. Genet.* **166**, 276–289 (2014).
- 779 14. Wright, C. F. *et al.* Genetic diagnosis of developmental disorders in the DDD study: A
780 scalable analysis of genome-wide research data. *Lancet* **385**, 1305–1314 (2015).
- 781 15. Hoyer, J. *et al.* Haploinsufficiency of ARID1B, a member of the SWI/SNF-A chromatin-
782 remodeling complex, is a frequent cause of intellectual disability. *Am. J. Hum. Genet.* **90**,
783 565–572 (2012).
- 784 16. Halgren, C. *et al.* Corpus callosum abnormalities, intellectual disability, speech
785 impairment, and autism in patients with haploinsufficiency of ARID1B. *Clin. Genet.* **82**,
786 248–255 (2012).
- 787 17. Roak, B. J. O. *et al.* Multiplex Targeted Sequencing Identifies Recurrently Mutated Genes
788 in Autism Spectrum Disorders. *Science (80-.)* **23**, 1619–1623 (2012).
- 789 18. Satterstrom, F. K. *et al.* Large-Scale Exome Sequencing Study Implicates Both
790 Developmental and Functional Changes in the Neurobiology of Autism. *Cell* **180**, 568–
791 584.e23 (2020).
- 792 19. Fitzgerald, T. W. *et al.* Large-scale discovery of novel genetic causes of developmental
793 disorders. *Nature* **519**, 223–228 (2015).
- 794 20. Celen, C. *et al.* \textit{Arid1b} haploinsufficient mice reveal neuropsychiatric phenotypes
795 and reversible causes of growth impairment. *Elife* **6**, e25730 (2017).
- 796 21. Karczewski, K. J. *et al.* The mutational constraint spectrum quantified from variation in
797 141,456 humans. *Nature* **581**, 434–443 (2020).
- 798 22. Clapier, C. R., Iwasa, J., Cairns, B. R. & Peterson, C. L. Mechanisms of action and
799 regulation of ATP-dependent chromatin-remodelling complexes. *Nat. Rev. Mol. Cell Biol.*
800 **18**, 407–422 (2017).
- 801 23. Ho, L. *et al.* EsBAF facilitates pluripotency by conditioning the genome for LIF/STAT3
802 signalling and by regulating polycomb function. *Nat. Cell Biol.* **13**, 903–913 (2011).
- 803 24. King, H. W. & Klose, R. J. The pioneer factor OCT4 requires the chromatin remodeller
804 BRG1 to support gene regulatory element function in mouse embryonic stem cells. *Elife*
805 **6**, 1–24 (2017).
- 806 25. Miller, E. L. *et al.* TOP2 synergizes with BAF chromatin remodeling for both resolution
807 and formation of facultative heterochromatin. *Nat. Struct. Mol. Biol.* **24**, 1–11 (2017).
- 808 26. Hodges, H. C. *et al.* Dominant-negative SMARCA4 mutants alter the accessibility
809 landscape of tissue-unrestricted enhancers. *Nat. Struct. Mol. Biol.* **25**, 61–72 (2018).
- 810 27. Iurlaro, M. *et al.* Mammalian SWI / SNF continuously restores local accessibility to
811 chromatin. *Nat. Genet.* (2021). doi:10.1038/s41588-020-00768-w
- 812 28. Schick, S. *et al.* Acute BAF perturbation causes immediate changes in chromatin
813 accessibility. *Nat. Genet.* **53**, (2021).
- 814 29. Weber, C. M. *et al.* *msWI/SNF promotes Polycomb repression both directly and through*
815 *genome-wide redistribution*. *Nature Structural and Molecular Biology* **28**, (Springer US,

- 816 2021).
- 817 30. Kia, S. K., Gorski, M. M., Giannakopoulos, S. & Verrijzer, C. P. SWI/SNF Mediates
818 Polycomb Eviction and Epigenetic Reprogramming of the INK4b-ARF-INK4a Locus.
819 *Mol. Cell. Biol.* **28**, 3457–3464 (2008).
- 820 31. Wilson, B. G. *et al.* Epigenetic antagonism between polycomb and SWI/SNF complexes
821 during oncogenic transformation. *Cancer Cell* **18**, 316–328 (2010).
- 822 32. Stanton, B. Z. *et al.* Smarca4 ATPase mutations disrupt direct eviction of PRC1 from
823 chromatin. *Nat. Publ. Gr.* **49**, 282–288 (2016).
- 824 33. Kadoc, C. *et al.* Dynamics of BAF – Polycomb complex opposition on heterochromatin
825 in normal and oncogenic states. *Nat. Genet.* **49**, 213–222 (2016).
- 826 34. Braun, S. M. G. *et al.* Rapid and reversible epigenome editing by endogenous chromatin
827 regulators. *Nat. Commun.* **8**, (2017).
- 828 35. Ni, K. *et al.* LSH mediates gene repression through macroH2A deposition. *Nat. Commun.*
829 **11**, (2020).
- 830 36. Zákány, J., Fromental-Ramain, C., Warot, X. & Duboule, D. Regulation of number and
831 size of digits by posterior Hox genes: A dose-dependent mechanism with potential
832 evolutionary implications. *Proc. Natl. Acad. Sci. U. S. A.* **94**, 13695–13700 (1997).
- 833 37. Quinonez, S. C. & Innis, J. W. Human HOX gene disorders. *Mol. Genet. Metab.* **111**, 4–
834 15 (2014).
- 835 38. Shibutani, M. *et al.* Arid1b haploinsufficiency causes abnormal brain gene expression and
836 autism-related behaviors in mice. *Int. J. Mol. Sci.* **18**, (2017).
- 837 39. Catela, C., Shin, M. M., Lee, D. H., Liu, J. P. & Dasen, J. S. Hox Proteins Coordinate
838 Motor Neuron Differentiation and Connectivity Programs through Ret/Gfra Genes. *Cell
839 Rep.* **14**, 1901–1915 (2016).
- 840 40. Mendelsohn, A. I., Dasen, J. S. & Jessell, T. M. Divergent Hox Coding and Evasion of
841 Retinoid Signaling Specifies Motor Neurons Innervating Digit Muscles. *Neuron* **93**, 792–
842 805.e4 (2017).
- 843 41. Jung, E. M. *et al.* Arid1b haploinsufficiency disrupts cortical interneuron development and
844 mouse behavior. *Nat. Neurosci.* **20**, 1694–1707 (2017).
- 845 42. Smith, A. L., Jung, E. M., Jeon, B. T. & Kim, W. Y. Arid1b haploinsufficiency in
846 parvalbumin- or somatostatin-expressing interneurons leads to distinct ASD-like and ID-
847 like behavior. *Sci. Rep.* **10**, 1–13 (2020).
- 848 43. Ellegood, J. *et al.* Neuroanatomy and behavior in mice with a haploinsufficiency of AT-
849 rich interactive domain 1B (ARID1B) throughout development. *Mol. Autism* **12**, 1–24
850 (2021).
- 851 44. Moffat, J. J. *et al.* Differential roles of ARID1B in excitatory and inhibitory neural
852 progenitors in the developing cortex. *Sci. Rep.* **11**, 1–17 (2021).
- 853 45. Walsh, J. J. *et al.* Systemic enhancement of serotonin signaling reverses social deficits in
854 multiple mouse models for ASD. *Neuropsychopharmacology* (2021). doi:10.1038/s41386-
855 021-01091-6
- 856 46. Morrill, S. A. & Amon, A. Why haploinsufficiency persists. *Proc. Natl. Acad. Sci. U. S. A.*
857 **116**, 11866–11871 (2019).
- 858 47. Wenderski, W. *et al.* Loss of the neural-specific BAF subunit ACTL6B relieves repression
859 of early response genes and causes recessive autism. *Proc. Natl. Acad. Sci. U. S. A.* **117**,
860 10055–10066 (2020).
- 861 48. Aizawa, H. *et al.* Dendrite Development Regulated by CREST, a Calcium-Regulated

- 862 Transcriptional Activator. *Science* (80-). **303**, 197–203 (2004).
 863 49. Vasileiou, G. *et al.* Chromatin-Remodeling-Factor ARID1B Represses Wnt/β-Catenin
 864 Signaling. *Am. J. Hum. Genet.* **97**, 445–456 (2015).
 865 50. Liu, X. *et al.* De Novo ARID1B mutations cause growth delay associated with aberrant
 866 Wnt/β–catenin signaling. *Hum. Mutat.* **41**, 1012–1024 (2020).
 867 51. Nagl, N. G., Wang, X., Patsialou, A., Van Scy, M. & Moran, E. Distinct mammalian
 868 SWI/SNF chromatin remodeling complexes with opposing roles in cell-cycle control.
 869 *EMBO J.* **26**, 752–763 (2007).
 870 52. Mah, K. M. & Weiner, J. A. Regulation of Wnt signaling by protocadherins. *Semin. Cell*
 871 *Dev. Biol.* **69**, 158–171 (2017).
 872 53. Xi, Q., He, W., Zhang, X. H. F., Le, H. Van & Massague, J. Genome-wide impact of the
 873 BRG1 SWI/SNF chromatin remodeler on the transforming growth factor β transcriptional
 874 program. *J. Biol. Chem.* **283**, 1146–1155 (2008).
 875 54. He, W. *et al.* Hematopoiesis Controlled by Distinct TIF1γ and Smad4 Branches of the
 876 TGFβ Pathway. *Cell* **125**, 929–941 (2006).
 877 55. Gao, F. *et al.* Heterozygous Mutations in SMARCA2 Reprogram the Enhancer Landscape
 878 by Global Retargeting of Article Heterozygous Mutations in SMARCA2 Reprogram the
 879 Enhancer Landscape by Global Retargeting of SMARCA4. *Mol. Cell* 1–14 (2019).
 880 doi:10.1016/j.molcel.2019.06.024
 881 56. Baek, S. *et al.* Bivariate Genomic Footprinting Detects Changes in Resource Bivariate
 882 Genomic Footprinting Detects Changes in Transcription Factor Activity. *Cell Reports* **19**,
 883 1710–1722 (2017).
 884 57. Corces, M. R. *et al.* The chromatin accessibility landscape of primary human cancers.
 885 *Science* (80-). **362**, eaav1898 (2018).
 886 58. Kennison, J. A. & Tamkun, J. W. Dosage-dependent modifiers of Polycomb and
 887 Antennapedia mutations in Drosophila. *Proc. Natl. Acad. Sci. U. S. A.* **85**, 8136–8140
 888 (1988).
 889 59. Schuettengruber, B., Bourbon, H., Croce, L. Di & Cavalli, G. Review Genome Regulation
 890 by Polycomb and Trithorax : 70 Years and Counting. *Cell* **171**, 34–57 (2017).
 891 60. Bernstein, B. E. *et al.* A Bivalent Chromatin Structure Marks Key Developmental Genes
 892 in Embryonic Stem Cells. *Cell* **125**, 315–326 (2006).
 893 61. Mazzoni, E. O. *et al.* Saltatory remodeling of Hox chromatin in response to rostrocaudal
 894 patterning signals. *Nat. Neurosci.* **16**, 1191–1198 (2013).
 895 62. Flajollet, S., Lefebvre, B., Cudejko, C., Staels, B. & Lefebvre, P. The core component of
 896 the mammalian SWI/SNF complex SMARCD3/BAF60c is a coactivator for the nuclear
 897 retinoic acid receptor. *Mol. Cell. Endocrinol.* **270**, 23–32 (2007).
 898 63. Yamamichi, N. *et al.* Cdx2 and the Brm-type SWI/SNF complex cooperatively regulate
 899 villin expression in gastrointestinal cells. *Exp. Cell Res.* **315**, 1779–1789 (2009).
 900 64. Wang, K. *et al.* Brg1 is required for Cdx2-mediated repression of Oct4 expression in
 901 mouse blastocysts. *PLoS One* **5**, (2010).
 902 65. Blackledge, N. P. & Klose, R. J. The molecular principles of gene regulation by Polycomb
 903 repressive complexes. *Nat. Rev. Mol. Cell Biol.* **0123456789**, (2021).
 904 66. Huang, Z. Q., Li, J., Sachs, L. M., Cole, P. A. & Wong, J. A role for cofactor-cofactor and
 905 cofactor-histone interactions in targeting p300, SWI/SNF and Mediator for transcription.
 906 *EMBO J.* **22**, 2146–2155 (2003).
 907 67. Ogiwara, H. *et al.* Histone acetylation by CBP and p300 at double-strand break sites

- 908 facilitates SWI/SNF chromatin remodeling and the recruitment of non-homologous end
909 joining factors. *Oncogene* **30**, 2135–2146 (2011).
- 910 68. Alver, B. H. *et al.* The SWI/SNF chromatin remodelling complex is required for
911 maintenance of lineage specific enhancers. *Nat. Commun.* **8**, (2017).
- 912 69. Wu, J. I., Lessard, J. & Crabtree, G. R. Understanding the Words of Chromatin
913 Regulation. *Cell* **136**, 200–206 (2009).
- 914 70. Mashtalir, N. *et al.* A Structural Model of the Endogenous Human BAF Complex Informs
915 Disease Mechanisms. *Cell* **183**, 802-817.e24 (2020).
- 916 71. Pan, J. *et al.* The ATPase module of mammalian SWI/SNF family complexes mediates
917 subcomplex identity and catalytic activity-independent genomic targeting. *Nat. Genet.* **51**,
918 618–626 (2019).
- 919 72. Wang, W. *et al.* Diversity and specialization of mammalian SWI / SNF complexes. *Genes*
920 *Dev.* **10**, 2117–2130 (1996).
- 921 73. Wang, W. *et al.* Purification and biochemical heterogeneity of the mammalian SWI-SNF
922 complex. *EMBO J.* **15**, 5370–5382 (1996).
- 923 74. Staahl, B. T. *et al.* Kinetic analysis of npBAF to nBAF switching reveals exchange of
924 SS18 with CREST and integration with neural developmental pathways. *J. Neurosci.* **33**,
925 10348–10361 (2013).
- 926 75. Shi, H. *et al.* ARID1A loss in neuroblastoma promotes the adrenergic-to-mesenchymal
927 transition by regulating enhancer-mediated gene expression. *Sci. Adv.* **6**, 1–13 (2020).
- 928 76. Huang, H. S. *et al.* Topoisomerase inhibitors unsilence the dormant allele of Ube3a in
929 neurons. *Nature* **481**, 185–191 (2012).
- 930 77. Doench, J. G. *et al.* Optimized sgRNA design to maximize activity and minimize off-
931 target effects of CRISPR-Cas9. *Nat. Biotechnol.* **34**, 184–191 (2016).
- 932 78. Sanson, K. R. *et al.* Optimized libraries for CRISPR-Cas9 genetic screens with multiple
933 modalities. *Nat. Commun.* **9**, 1–15 (2018).
- 934 79. Meers, M. P., Bryson, T. D., Henikoff, J. G. & Henikoff, S. Improved CUT&RUN
935 chromatin profiling tools. *Elife* **8**, 1–16 (2019).
- 936 80. Frankish, A. *et al.* GENCODE reference annotation for the human and mouse genomes.
937 *Nucleic Acids Res.* **47**, D766–D773 (2019).
- 938 81. Bray, N. L., Pimentel, H., Melsted, P. & Pachter, L. Near-optimal probabilistic RNA-seq
939 quantification. *Nat. Biotechnol.* **34**, 525–527 (2016).
- 940 82. Soneson, C., Love, M. I. & Robinson, M. D. Differential analyses for RNA-seq:
941 transcript-level estimates improve gene-level inferences. *F1000Research* **4**, 1521 (2015).
- 942 83. Love, M. I., Huber, W. & Anders, S. Moderated estimation of fold change and dispersion
943 for RNA-seq data with DESeq2. *Genome Biol.* **15**, 550 (2014).
- 944 84. Stephens, M. False discovery rates: A new deal. *Biostatistics* **18**, 275–294 (2017).
- 945 85. Kuleshov, M. V *et al.* Enrichr : a comprehensive gene set enrichment analysis web server
946 2016 update. *Nucleic Acids Res.* **44**, 90–97 (2016).
- 947 86. Mi, H., Muruganujan, A. & Thomas, P. D. PANTHER in 2013: Modeling the evolution of
948 gene function, and other gene attributes, in the context of phylogenetic trees. *Nucleic*
949 *Acids Res.* **41**, 377–386 (2013).
- 950 87. Marcel, M. Cutadapt removes adapter sequences from high-throughput sequencing reads.
951 *EMBnet. J.* **17**, 10–12 (2011).
- 952 88. Langmead, B. & Salzberg, S. L. Fast gapped-read alignment with Bowtie 2. *Nat. Methods*
953 **9**, 357–359 (2012).

- 954 89. Li, H. *et al.* The Sequence Alignment/Map format and SAMtools. *Bioinformatics* **25**,
955 2078–2079 (2009).
- 956 90. Buenrostro, J. D., Giresi, P. G., Zaba, L. C., Chang, H. Y. & Greenleaf, W. J.
957 Transposition of native chromatin for fast and sensitive epigenomic profiling of open
958 chromatin, DNA-binding proteins and nucleosome position. *Nat. Methods* **10**, 1213–1218
959 (2013).
- 960 91. Zhang, Y. *et al.* Model-based Analysis of ChIP-Seq (MACS). (2008). doi:10.1186/gb-
961 2008-9-9-r137
- 962 92. Quinlan, A. R. & Hall, I. M. BEDTools: A flexible suite of utilities for comparing
963 genomic features. *Bioinformatics* **26**, 841–842 (2010).
- 964 93. McLean, C. Y. *et al.* GREAT improves functional interpretation of cis-regulatory regions.
965 *Nat. Biotechnol.* **28**, 495–501 (2010).
- 966 94. Heinz, S. *et al.* Simple Combinations of Lineage-Determining Transcription Factors Prime
967 cis-Regulatory Elements Required for Macrophage and B Cell Identities. *Mol. Cell* **38**,
968 576–589 (2010).
- 969 95. Ramírez, F. *et al.* deepTools2: a next generation web server for deep-sequencing data
970 analysis. *Nucleic Acids Res.* **44**, W160–W165 (2016).
- 971 96. Fornes, O. *et al.* JASPAR 2020: Update of the open-Access database of transcription
972 factor binding profiles. *Nucleic Acids Res.* **48**, D87–D92 (2020).
- 973 97. Grant, C. E., Bailey, T. L. & Noble, W. S. FIMO: Scanning for occurrences of a given
974 motif. *Bioinformatics* **27**, 1017–1018 (2011).
- 975
- 976

Supplementary Files

This is a list of supplementary files associated with this preprint. Click to download.

- [SupplementaryData1.pdf](#)
- [SupplementaryFigures.docx](#)